A Novel Method of Obtaining Cell Membrane Permeability Parameters Using Non-Ideal Thermodynamic Assumptions

by

Laura Adeline Gabler Pizarro

A thesis submitted in partial fulfillment of the requirements for the degree of

Master of Science

in

Chemical Engineering

Department of Chemical and Materials Engineering
University of Alberta

Abstract

Cryopreservation is the storage of biological matter at subzero temperatures to preserve it. As one can imagine, this comes with many challenges, including exposure to high solute concentrations as pure water in the extracellular solution freezes, cell dehydration as the intracellular water leaves the cells when the extracellular solution becomes hypertonic, intracellular ice formation, and more. These effects can be mitigated by optimizing the cooling rate, which depends on the cells' permeability to water, and adding cryoprotective agents (CPAs) to the solutions. CPAs can be non-permeating or permeating, and for the latter, the permeability of the cells to CPAs also becomes an important factor. Mathematical modelling of the cryopreservation process is a useful tool to investigate all the different variables that effect the results of this process. To successfully design a cryopreservation protocol, the changing cell volume during cryopreservation can be modelled by obtaining cell-specific parameters that impact the cell volume, namely L_p which is the permeability of the cell membrane to water, P_s which is the permeability of the cell membrane to CPA, and the osmotically inactive fraction, b, which is the intracellular volume fraction that cannot leave the cells. These parameters have been found previously for different cell types under ideal and dilute assumptions, but biological solutions at subzero temperatures are far from ideal and dilute, especially when CPAs are included. The osmotic virial equation can be used to model the changing cell volume under non-ideal assumptions, and the intracellular environment is described using the grouped solute, which consists of all impermeant intracellular solutes grouped together. Therefore, two additional cell-specific parameters are required to model the cell volume during cryopreservation under non-ideal assumptions, which are the second and third osmotic virial coefficients of this grouped solute, B_{gg} and C_{ggg}.

In this work, a novel fitting method is presented where kinetic cell volume data with 5x phosphate buffered saline (PBS) solution is used to fit for L_p^* and b^* (the asterisks indicating that these properties are obtained with non-ideal assumptions), and kinetic cell volume data with 3 molal dimethyl sulfoxide (DMSO) is used to fit for B_{gg}, C_{ggg}, and P_s^*. Because the fitting for L_p^* and b^* requires the parameters B_{gg} and C_{ggg}, the fitting process is done iteratively between both types of data, starting with $B_{gg} = C_{ggg} = 0$. The iterative process converges to the final five cell-specific parameters. This was done for human umbilical vein endothelial cells (HUVECs) and H9C2 rat cardiomyocytes at room temperature. Additionally, the temperature dependence of L_p^* and P_s^* are obtained by using the parameters found from the new fitting method at room temperature to fit kinetic cell volume data with 5x PBS at 4 °C to obtain b_{4C}^* and E_{aL_p} which is the activation energy of L_p^*, and to fit kinetic cell volume data with 3 molal DMSO at 4 °C to obtain E_{aP_s} which is the activation energy of P_s^*. This novel fitting method can be used to efficiently determine the five cell-specific fitting parameters, and the temperature dependence of the permeability parameters, required to model the changing cell volume during cryopreservation, an asset that will greatly impact the design of cryopreservation protocols.

Preface

This work, with modifications, is being prepared for submission as: Gabler Pizarro, L. A., McGann, L. E., Elliott, J. A. W. “A Novel Method of Obtaining Cell Membrane Permeability Parameters Using Non-Ideal Thermodynamic Assumptions”.

Papiamento: E logro aki ta dedica na mi mayornan, Evelyne Ponson y Juan Carlos Gabler Pizarro. Danki pa semper support mi sonjonan y pa pushami pa logra nan. Sin boso, esaki lo no ta posibel.

English: This achievement is dedicated to my parents, Evelyne Ponson and Juan Carlos Gabler Pizarro. Thank you for always supporting my dreams and pushing me to achieve them. Without you, this would not be possible.

Acknowledgements

I would like to express my sincerest gratitude and appreciation to my supervisor, Dr. Janet Elliott. Thank you for trusting me with this project and guiding me through all the obstacles we encountered.

To Dr. Locksley McGann, thank you for your wisdom, guidance, and incredible stories. I feel honored to have been able to work with you on this project.

To Dr. Leah Marquez-Curtis, thank you for teaching me everything I know about culturing cells, always being there when I needed you to look at something I thought was weird under the microscope, and most importantly, thank you for your friendship.

To my group members, Elham Ashrafi, Hikmat Binyaminov, and Soheil Rezvani. Thank you for your friendship and your MATLAB tips and tricks.

To my parents, Evelyne Ponson and Juan Carlos Gabler Pizarro, my brother, Alan Gabler Pizarro, and my niece and nephew, Vanellope and Alexander Gabler Pizarro. Thank you for always believing in me and being there with open arms at the airport every time. You will always be my home.

To my boyfriend, Gilmar Arends, thank you for your endless support and patience. Who would have thought we would end up here in the freezing cold together after so many adventures? I look forward to the many adventures we will experience together in the future.

Finally, I would like to thank God, for leading me on this path, giving me the courage to move across the world to achieve this dream, and always being with me, “even to the end of the age”.

Table of Contents

List of Tables

List of Figures

Chapter 1. Introduction

1.1. Background

1.1.1. Cryobiology

Cryobiology has been a field with growing interest over the past century due to its application in areas such as tissue engineering[1], gene storage of endangered species[2], and reproductive medicine.[3] During cryopreservation, biological matter is preserved by storing it at temperatures below zero degrees Celsius. At these temperatures, metabolic reactions are slowed down, which essentially slows down time for that biological matter.[4] As one can imagine, this comes with many obstacles because these cells and tissues are exposed to environments that are far from their natural state. When cells are brought to temperatures below freezing, water in the intra- and extracellular environment can begin to solidify. Not only does this expose the cells to mechanical stresses caused by the formation of ice, but the remaining unfrozen solution becomes more concentrated, which can result in osmotic stress.

Cells are in osmotic equilibrium with the extracellular space when the solution is isotonic. As the temperature is decreased during the cryopreservation process, water in the extracellular solution solidifies to pure ice, leaving the total solutes behind in a smaller solvent volume, and thus a hypertonic solution.[4] This deviation from osmotic equilibrium will result in water leaving the cells through their semi-permeable membranes until the equilibrium is reestablished. As water leaves the cells, the intracellular environment also becomes more concentrated, which decreases the freezing point of the intracellular solution.[4] To the cells' benefit, this reduces the risk of intracellular ice formation. The rate at which water leaves the cells is dependent on the permeability of the cells to water, which varies among different cell types. If the temperature is decreased rapidly, the extracellular increase in concentration can be faster than the rate that water

is able to leave the cells allowing the temperature to drop below the intracellular freezing point, which increases the risk of intracellular ice formation. On the other hand, cooling the cells too slowly will result in the cells being exposed to high solute concentrations for a long time and becoming dehydrated.[4–6] This creates an optimum cooling rate that is different for each cell type, depending on the cell's permeability to water.

1.1.2. Cryoprotective Agents

Cryoprotective agents (CPAs) are used to reduce the injuries sustained during cryopreservation. Non-permeating CPAs are large compounds that are not able to pass through the cell membrane, and thus draw water out of cells reducing the cell volume before undergoing the cryopreservation process. This increases the intracellular concentration before freezing, which reduces the risk of intracellular freezing.[4] In other words, non-permeating CPAs reduce injuries caused by fast cooling. Permeating CPAs are smaller molecules that can pass through the cell membrane and reduce the freezing point of the intra- and extracellular environment. The freezing point reduction will result in a greater unfrozen volume at lower temperatures, which reduces the solute concentration at these temperatures. In other words, permeating CPAs reduce injuries caused by slow cooling.[4] Both types of CPAs expand the range of the optimal cooling rate and improve cell viability during cryopreservation.

The additional aspect to consider when working with CPAs is the cell injury caused by these CPAs. During addition and removal, the intra- and extracellular changes in osmolality can lead to the cells shrinking or swelling beyond a tolerable size, where the cells dehydrate or burst. Specifically, during the removal of a permeating CPA after thawing by placing the cells directly into an isotonic solution, the higher osmolality from the CPA inside the cells will force water into

the intracellular space. This leads to the need for gradual post-thaw CPA removal or the use of non-permeating CPAs to help reduce the osmotic pressure gradient between the intra- and extracellular space during permeating CPA removal.[7] Additionally, exposing the cells to these compounds, specifically permeating CPAs, can result in other injuries. Permeating CPA have been found to have damaging effects on mitochondria, proteins, epigenetics, and more. The exact mechanisms and lasting effects of CPA toxicity at these molecular levels are complex and hypothetical, therefore much research is still needed.[7]

Several studies have found that the combination of different CPAs helps lower the toxic effects and that lower concentrations of CPAs at lower temperatures for a shorter amount of time results in less damage.[8–11] However, to know if the permeating CPA has equilibrated between the inside and outside of the cells, the cell's permeability to CPAs must be known. Subsequently, the cryopreservation protocol can be designed to minimize the time the cells are exposed to these CPAs. Additionally, the CPA permeability is known to be temperature dependent, thus if the toxicity is to be reduced by adding the CPAs at temperatures close to 0 °C, the temperature dependence of the CPA permeability must also be known. This is especially important because glycerol, which is a permeating CPA at higher temperatures, has been found to behave as a non-permeating CPA if it is added at temperatures closer to 0 °C.[12] Studies that have found activation energies for the permeability of glycerol show that it is larger than the activation energies of other commonly used permeating CPAs.[13,14] However, a recent study found that because glycerol is not as toxic as other commonly used permeating CPAs, such as dimethyl sulfoxide (DMSO), adding glycerol to the cells and allowing the intra- and extracellular environments to reach equilibrium at room temperature results in similar cell viabilities to those found when adding DMSO at 0 °C.[15] This illustrates the importance of knowing how the permeability of CPAs varies with temperature.

1.1.3. Cell Permeability and Cell Volume Modelling

When designing a cryopreservation procedure, there are many variables that need to be considered, as many of these variables can lead to cryoinjury. The cooling rate and if it is constant or not, the types and amounts of CPAs used, when and how the CPAs are added and removed, are just a few variables to consider. Conducting experiments to test all the possible choices for these variables would be endless. A faster and more efficient way to deal with all these variables is to simulate the cryopreservation process by using mathematical models which require much less experimentation. Specifically, thermodynamic models have been used to find cell-specific parameters that are required to know how cells will respond when undergoing cryopreservation.[16–21] These models, including the one described in further detail in Section 1.2., allow for the prediction of the changing cell volume by fitting kinetic cell volume data to find the permeability parameters of specific cell types. Many of these studies, however, assumed that the solutions are ideal and dilute, but the intra- and extracellular solutions during cryopreservation can reach a high concentration, and thus assuming the solutions are ideal and dilute could result in severe errors in these permeability parameters.[22,23] The Elliott et al. form of the McMillan and Mayer[24] osmotic virial equation has been used to account for the non-ideality of the biological solutions involved during cryopreservation.[23,25–28] The osmotic virial equation considers the interactions between molecules of the same solute, while Elliott et al.'s form also considers interactions between molecules of different solutes. Normally, this would require fitting to experimental data of multi-solute interactions, but Elliott et al. proposed a more efficient way that only requires single-solute data.[25,28]

The Elliott et al. form of the osmotic virial equation allows us to more accurately represent both the intra- and extracellular solutions by not assuming they are ideal and dilute during the

entire cryopreservation process. However, to use this equation, the exact contents of the intracellular solution must be known, which brings forward its own problems. In order to solve this issue, studies have used a grouped solute assumption, combining all non-permeating intracellular solutes into one.[22,23] Ross-Rodriguez et al. used the grouped solute assumption to fit non-permeating cell volume data using the osmotic virial equation truncated to the second degree due to lacking in sufficient data at high osmolalities to fit to a higher degree. They found that a number of cells, including human umbilical vein endothelial cells (HUVECs), do not behave in an ideal manner, resulting in inaccurate cell volume modelling especially at higher osmolalities of non-permeating solutes.[22] More recently, Zielinksi et al. proposed a novel method to fit for the second and third osmotic virial coefficient of this grouped solute, B_{gg} and C_{ggg}, respectively, for HUVECs with equilibrium cell volume data at different and high enough osmolalities of non-permeating and permeating solutes to fit to a third degree osmotic virial equation. They showed that the second osmotic virial coefficient, B_{gg}, is not sensitive to non-permeating solute data, but becomes much more relevant to the model when permeating solutes are involved. By fitting B_{gg} to permeating solute cell volume data, the precision of the model is improved. Additionally, including the third order fit resulted in more accurate equilibrium data modelling.[23] However, Zielinksi et al.'s work only focused on equilibrium cell volume data, which allows for the measurement of the osmotic virial coefficients of the intracellular grouped solute, but not the water and cryoprotectant permeability parameters, L_p^* and P_s^*, respectively, which require kinetic cell volume data.

Many different techniques for kinetic cell volume measurements have been developed over the years. These can generally be categorized in two groups, which are techniques for large cell samples and small cell samples. Each technique has their advantages and disadvantages. Mainly,

for techniques requiring large cell samples the pool of cell sizes is well distributed and many cells can be measured in a short time, but this requires a large number of cells, which is not feasible for some cell types, and cells cannot be analyzed individually. On the other hand, for techniques requiring a small cell sample, the disadvantages for techniques using large cell samples become the advantages, meaning cell types that are harder to come by can be analyzed using a small sample size and these analyses can be done on individual cells. However, the cell distribution is small, because a small number of cells can be analyzed at a time compared to the techniques requiring large cell samples.[29] Additionally, because of the small volumes used and the inability to adequately mix the extracellular solution, the important assumption that is made when modelling changing cell volume concerning the constant extracellular osmolality is made more difficult, and caution must be had when using these techniques with respect to this assumption. Some examples of large cell sample volume measurement techniques include macroscopic stopped-flow systems[30,31] and electronic particle size counters.[21,32,33] Some examples of small cell sample volume measurement techniques are microscopic stopped-flow techniques,[34] micropipette perfusion techniques,[35] and microperfusion chamber methods.[36] In the present work, the method used for cell volume measurements uses an electronic particle size counter, and the mechanism of this particle size counter is detailed in Section 2.1.3.

1.1.4. Human Umbilical Vein Endothelial Cells (HUVECs) and H9C2 Cardiomyocytes

In this work, kinetic cell volume data in hypertonic conditions and isotonic cell volume data are obtained for human umbilical vein endothelial cells (HUVECs) and H9C2 rat cardiomyocytes because these cells were of interest for the Elliott/McGann research group at the time of completing this work and were readily available in the laboratory. HUVECs are a popular

model cell when researching the endothelium of blood vessels, and a successful cryopreservation procedure for HUVECs is vital due to the role these play in the tissue engineering of vascular tissues.[37] H9C2 cells are rat heart muscle cells derived from embryonic rat hearts. They are frequently used due to how similar they are to skeletal muscle cells and their ability to beat as cardiac muscle cells would in the presence of electrical stimulus or acetylcholine.[38] These cells were chosen as example cells to be used in this work, but any other cells could have been chosen as examples.

1.2. Governing Equations

In this work, the changing cell volume is modelled by fitting the equations described in a previous study to kinetic cell volume data.[23] The equations in this previous study are modified with the specific notations used in this work, and they are briefly explained in this section.

The cell volume changes that result from the transport of water and permeating solutes during cryopreservation can be modelled using the following equations[6,16,23]

$$\frac{dV_w}{dt} = L_p^* A_{cell}(t) RT \rho_w \left[\pi^{in}(t) - \pi^{ex}\right] \quad (1)$$

and

$$\frac{dV_p}{dt} = P_s^* A_{cell}(t) \left[a_p^{ex} - a_p^{in}(\mathrm{t})\right], \quad (2)$$

where V_w and V_P are the volume of water and volume of cryoprotectant inside the cell, respectively, L_p^* is the hydraulic conductivity, P_s^* is the membrane permeability to permeating solutes or cryoprotectants, R is the gas constant, T is the temperature, ρ_w is the density of water, π^{in} and π^{ex}

are the intra- and extracellular osmolalities, respectively, a_p^{in} and a_p^{ex} are the intra- and extracellular activity of cryoprotectants, respectively, and A_{cell} is the surface area of the cell. The values obtained for L_p^* and P_s^* in this work are not comparable to values obtained for L_p and P_s in other works that use the ideal and dilute equations because those equations are different and consider a different driving force, therefore the asterisk is added to highlight the differences. L_p^* and P_s^* are assumed to be temperature dependent with an Arrhenius behaviour, and are thus described using the following equations, respectively,

$$L_p^* = L_p^{*RT} \exp\left[\frac{E_{aL_p}}{R}\left(\frac{1}{T_{RT}} - \frac{1}{T}\right)\right] \tag{3}$$

and

$$P_s^* = P_s^{*RT} \exp\left[\frac{E_{aP_s}}{R}\left(\frac{1}{T_{RT}} - \frac{1}{T}\right)\right] \tag{4}$$

where L_p^{*RT} and P_s^{*RT} are the reference points used of L_p^* and P_s^* at room temperature, T_{RT}, and E_{aL_p} and E_{aP_s} are the respective activation energies. A_{cell} is assumed to change with the volume of the assumed spherical cells as

$$A_{cell}(t) = 4\pi\left[\frac{3}{4\pi}V_{cell}(t)\right]^{2/3}, \tag{5}$$

where V_{cell} is the total cell volume and is calculated as

$$V_{cell}(t) = V_w(t) + V_p(t) + b^*V_0\,, \tag{6}$$

where V_0 is the isotonic cell volume and b^* is the osmotically inactive fraction of the cell, which is the fraction of the intracellular content that cannot leave the cell.

The multi-solute osmotic virial equation form by Elliott et al. non-ideally describes the intra- and extracellular chemical potentials of water and the cryoprotectant using the following equations[23,25–27]

$$\mu_W = \mu_W^0 - RTM_W\pi\,, \tag{7}$$

where π is the osmolality of the intra- or extracellular solution and is described as[23]

$$\pi = \sum_{i=2}^{r} k_i m_i + \sum_{i=2}^{r}\sum_{j=2}^{r}\left[\frac{(B_{ii}+B_{jj})}{2} k_i m_i k_j m_j\right] + \sum_{i=2}^{r}\sum_{j=2}^{r}\sum_{k=2}^{r}\left[(C_{iii}C_{jjj}C_{kkk})^{1/3} k_i m_i k_j m_j k_k m_k\right], \tag{8}$$

and

$$\mu_p = k_p\theta_p + RTk_p\left[ln\left(M_w m_p\right) + \sum_{i=2}^{r}\left[\left(B_{ii}+B_{pp}\right)k_i m_i\right] + \frac{3}{2}\sum_{i=2}^{r}\sum_{j=2}^{r}\left[(C_{iii}C_{jjj}C_{ppp})^{1/3} k_i m_i k_j m_j\right]\right], \tag{9}$$

where μ_W and μ_p are the chemical potentials of water and the cryoprotectant, respectively, μ_W^0 is the chemical potential of pure water, M_W is the molar mass of water, k_p and k_i are the dissociation constants of the cryoprotectant and solute *i*, respectively, θ_p is a function of temperature and pressure for the cryoprotectant, m_p and m_i are the molalities of the cryoprotectant and solute *i*, respectively, B_{pp} and B_{ii} are the second osmotic virial coefficients of the cryoprotectant and solute *i*, respectively, and C_{ppp} and C_{iii} are the third osmotic virial coefficients of the cryoprotectant and solute *i*, respectively.

The activity of the cryoprotectant can be described in terms of chemical potential using the following equation[23]

$$RTln(a_p) = \mu_p - \mu_p^0 , \tag{10}$$

where μ_p^0 is chemical potential of the cryoprotectant at a reference point. Equation 9 is inserted in Equation 10 to replace μ_p and taking μ_p^0 to be $k_p\theta_p$, the following equation for activity is obtained[23]

$$a_p = \exp\left[k_p\left[\ln(M_W m_p) + \sum_{i=2}^{r}\left[(B_{ii} + B_{pp})k_i m_i\right] + \frac{3}{2}\sum_{i=2}^{r}\sum_{j=2}^{r}\left[(C_{iii}C_{jjj}C_{ppp})^{1/3}k_i m_i k_j m_j\right]\right]\right]. \tag{11}$$

In this work, the solutes present in the extracellular space are a permeating cryoprotectant and sodium chloride from the phosphate buffered saline solution. The intracellular space also contains the permeating cryoprotectant and all compounds that are native to the cell. The compounds that are native to the cell are combined and assumed to be non-permeating and behave as one solute, the grouped solute, which is mentioned in Section 1.1.3. Thus, each of the intra- and extracellular space contain two solutes and Equations 8 and 11 become[23]

$$\begin{aligned}\pi^{in}(t) = {} & m_p^{in}(t) + m_g^{in}(t) + B_{pp}\left(m_p^{in}(t)\right)^2 + B_{gg}\left(m_g^{in}(t)\right)^2 \\ & + \left(B_{pp} + B_{gg}\right)m_p^{in}(t)m_g^{in}(t) + C_{ppp}\left(m_p^{in}(t)\right)^3 \\ & + 3\left(C_{ppp}^2 C_{ggg}\right)^{\frac{1}{3}}\left(m_p^{in}(t)\right)^2 m_g^{in}(t) + 3\left(C_{ppp}C_{ggg}^2\right)^{\frac{1}{3}}m_p^{in}(t)\left(m_g^{in}(t)\right)^2 \\ & + C_{ggg}\left(m_g^{in}\right)^3,\end{aligned} \tag{12}$$

$$\begin{aligned}\pi^{ex} = {} & m_p^{ex} + k_N m_N^{ex} + B_{pp}(m_p^{ex})^2 + B_{NN}(k_N m_N^{ex})^2 + (B_{pp} + B_{NN})m_p^{ex}k_N m_N^{ex} \\ & + C_{ppp}(m_p^{ex})^3 + 3(C_{ppp}^2 C_{NNN})^{1/3}(m_p^{ex})^2 k_N m_N^{ex} \\ & + 3(C_{ppp}C_{NNN}^2)^{1/3}m_p^{ex}(k_N m_N^{ex})^2 + C_{NNN}(k_N m_N^{ex})^3,\end{aligned} \tag{13}$$

$$a_p^{in}(t) = \exp\left[ln\left(M_w m_p^{in}(t)\right) + (B_{pp} + B_{gg})m_g^{in}(t) + \frac{3}{2}\left(C_{ggg}{}^2 C_{ppp}\right)^{1/3}\left(m_g^{in}(t)\right)^2\right], \tag{14}$$

and

$$a_p^{ex} = \exp\left[ln\left(M_w m_p^{ex}\right) + (B_{pp} + B_{NN})k_N m_N^{ex} + \frac{3}{2}\left(C_{NNN}{}^2 C_{ppp}\right)^{1/3}(k_N m_N^{ex})^2\right], \tag{15}$$

where the subscripts *p*, *g*, and *N*, represent the permeating cryoprotectant, the grouped solute, and sodium chloride, respectively, and the superscripts *in* and *ex* represent the intra- and extracellular space, respectively. In this work, the extracellular osmolality and activity are assumed to remain constant because the volume of the intracellular contents is negligible when compared to the volume of the extracellular solution. The intracellular molalities of the cryoprotectant and the grouped solute, m_p^{in} and m_g^{in}, vary as the volume of the cells change, thus a_p^{in} and π^{in} are time-dependent, and are described using the following equations

$$m_p^{in}(t) = \frac{V_p(t)\rho_p}{M_p V_W(t)\rho_W} \tag{16}$$

and

$$m_g^{in}(t) = \frac{N_g^0}{V_W(t)\rho_W}, \tag{17}$$

where ρ_p is the density of the cryoprotectant, M_p is the molar mass of the cryoprotectant, and N_g^0 is the number of moles of the grouped solutes inside the cell at isotonic conditions. The grouped solute is assumed to be non-permeating, thus N_g^0 remains constant and is expressed as

$$N_g^0 = m_g^0 V_0\,(1 - b^*)\rho_w\,, \tag{18}$$

where m_g^0 is the intracellular molality of the grouped solute at isotonic conditions and is described by solving Equation 8 for the intracellular environment at isotonic conditions:

$$\pi^0 = m_g^0 + B_{gg}(m_g^0)^2 + C_{ggg}(m_g^0)^3\,, \tag{19}$$

where π^0 is the intracellular osmolality at isotonic conditions.

The water[39] and CPA[40] densities are assumed to change with temperature and are calculated using these equations

$$\rho_w = 999.974950 \times 10^{-18}\left[1 - \frac{(T - 3.983035)^2(T + 301.797)}{522528.9(T + 69.34881)}\right] \tag{20}$$

and

$$\rho_p = -9.87181 \times 10^{-19}T + 1.11979 \times 10^{-15}\,, \tag{21}$$

where ρ_w and ρ_p are the densities of water and the CPA used in this work, dimethyl sulfoxide (DMSO), in $\frac{kg}{\mu m^3}$, and T is the temperature of the solution in ℃.

With the previous equations, the model has five remaining parameters that will be obtained when fitting the model to kinetic cell volume data, L_p^*, b^*, B_{gg}, C_{ggg}, and P_s^*. However, to decrease the number of parameters that are allowed to fit to experimental data, the previous equations can be modified to fit experimental data where the cells are only exposed to varying extracellular osmolalities and not a cryoprotectant. This will allow for the fitting of the previous equations to CPA-free data, meaning all parameters and variables relating to the CPA are removed from the model. The fitting parameters that remain in the model are L_p^*, b^*, B_{gg}, and C_{ggg}. However, a previous study found that B_{gg} and C_{ggg} are more sensitive in the presence of cryoprotectants,[23] thus fitting for these two coefficients along with P_s^* to the CPA data would deliver more accurate results. The equations used for the CPA and CPA-free data fittings are summarized in Table 1, and the variables, parameters, their descriptions and units used in this work are summarized in Table 2.

Table 1. Summary of equations used to model CPA and CPA-free data.[23]

Equations to model data where a permeating CPA is present	Equation Number
$\frac{dV_w}{dt} = L_p^* A_{cell}(t) RT \rho_w \left[\pi^{in}(t) - \pi^{ex}\right]$	(1)
$\frac{dV_P}{dt} = P_s^* A_{cell}(t) \left[a_p^{ex} - a_p^{in}(t)\right]$	(2)
$L_p^* = L_p^{RT} \exp\left[\frac{E_{aL_P}}{R}\left(\frac{1}{T_{RT}} - \frac{1}{T}\right)\right]$	(3)
$P_s^* = P_s^{RT} \exp\left[\frac{E_{aP_s}}{R}\left(\frac{1}{T_{RT}} - \frac{1}{T}\right)\right]$	(4)
$A_{cell}(t) = 4\pi\left[\frac{3}{4\pi}V_{cell}(t)\right]^{2/3}$	(5)
$V_{cell}(t) = V_w(t) + V_p(t) + b^* V_0$	(6)
$\pi^{in}(t) = m_p^{in}(t) + m_g^{in}(t) + B_{pp}\left(m_p^{in}(t)\right)^2 + B_{gg}\left(m_g^{in}(t)\right)^2 + \left(B_{pp} + B_{gg}\right)m_p^{in}(t)m_g^{in}(t) + C_{ppp}\left(m_p^{in}(t)\right)^3 + 3\left(C_{ppp}^2 C_{ggg}\right)^{\frac{1}{3}}\left(m_p^{in}(t)\right)^2 m_g^{in}(t) + 3\left(C_{ppp}C_{ggg}^2\right)^{\frac{1}{3}} m_p^{in}(t)\left(m_g^{in}(t)\right)^2 + C_{ggg}\left(m_g^{in}\right)^3$	(12)
$\pi^{ex} = m_p^{ex} + k_N m_N^{ex} + B_{pp}(m_p^{ex})^2 + B_{NN}(k_N m_N^{ex})^2 + (B_{pp} + B_{NN})m_p^{ex} k_N m_N^{ex} + C_{ppp}(m_p^{ex})^3 + 3(C_{ppp}^2 C_{NNN})^{1/3}(m_p^e)^2 k_N m_N^{ex} + 3(C_{ppp}C_{NNN}^2)^{1/3} m_p^{ex}(k_N m_N^{ex})^2 + C_{NNN}(k_N m_N^{ex})^3$	(13)
$a_p^{in}(t) = exp\left[ln\left(M_w m_p^{in}(t)\right) + (B_{pp} + B_{gg})m_g^{in}(t) + \frac{3}{2}\left(C_{ggg}{}^2 C_{ppp}\right)^{1/3}\left(m_g^{in}(t)\right)^2\right]$	(14)
$a_p^{ex} = exp\left[ln\left(M_w m_p^{ex}\right) + (B_{pp} + B_{NN})k_N m_N^{ex} + \frac{3}{2}\left(C_{NNN}{}^2 C_{ppp}\right)^{1/3}(k_N m_N^{ex})^2\right]$	(15)
$m_p^{in}(t) = \frac{V_p(t)\rho_p}{M_p V_W(t)\rho_W}$	(16)
$m_g^{in}(t) = \frac{N_g^0}{V_W(t)\rho_W}$	(17)

Table 1 continued.

Equations to model data where a permeating CPA is present	Equation Number
$N_g^0 = m_g^0 V_0\ (1 - b^*)\rho_w$	(18)
$\pi^0 = m_g^0 + B_{gg}(m_g^0)^2 + C_{ggg}(m_g^0)^3$	(19)
$\rho_w = 999.974950 \times 10^{-18}\left[1 - \frac{(T - 3.983035)^2(T + 301.797)}{522528.9(T + 69.34881)}\right]$	(20)[39]
$\rho_p = -9.87181 \times 10^{-19}T + 1.11979 \times 10^{-15}$	(21)[40]
Equations to model CPA-free data	**Equation Number**
$\frac{dV_w}{dt} = L_p^* A_{cell}(t) RT\rho_w\left(\pi^{in}(t) - \pi^{ex}\right)$	(1)
$L_p^* = L_p^{RT} \exp\left[\frac{E_{aL_P}}{R}\left(\frac{1}{T_{RT}} - \frac{1}{T}\right)\right]$	(3)
$A_{cell}(t) = 4\pi\left[\frac{3}{4\pi}V_{cell}(t)\right]^{2/3}$	(5)
$V_{cell}(t) = V_w(t) + b^* V_0$	(6)
$\pi^{in}(t) = m_g^{in}(t) + B_{gg}\left(m_g^{in}(t)\right)^2 + C_{ggg}\left(m_g^{in}\right)^3$	(12)
π^{ex} is a measured value with an osmometer.	(13)
$m_g^{in}(t) = \frac{N_g^0}{V_W(t)\rho_W}$	(17)
$N_g^0 = m_g^0 V_0\ (1 - b^*)\rho_w$	(18)
$\pi^0 = m_g^0 + B_{gg}(m_g^0)^2 + C_{ggg}(m_g^0)^3$	(19)
$\rho_w = 999.974950 \times 10^{-18}\left[1 - \frac{(T - 3.983035)^2(T + 301.797)}{522528.9(T + 69.34881)}\right]$	(20)[39]

Table 2. Variables and parameters used in this work's theoretical model with their descriptions, units, and values (if applicable), with DMSO as the cryoprotectant.[23]

Variables		
Symbol	*Description*	*Unit*
V_w	Intracellular volume of water	μm^3
V_p	Intracellular volume of the cryoprotectant	μm^3
V_{cell}	Total volume of the cell	μm^3
A_{cell}	Surface area of the cell	μm^2
T	Temperature, measured (when it varies, as in the low temperature runs)	K
ρ_w	Density of water, calculated with temperature dependence (when it varies, as in the low temperature runs) using Equation (20)[39]	$\frac{kg}{\mu m^3}$
ρ_p	Density of DMSO, calculated with temperature dependence (when it varies, as in the low temperature runs) using Equation (21)[40]	$\frac{kg}{\mu m^3}$
π^{in}	Intracellular osmolality	$\frac{Osm}{kg\ water}$
a_p^{in}	Intracellular activity of the cryoprotectant	
m_p^{in}	Intracellular molality of the cryoprotectant	$\frac{mol}{kg\ water}$
m_g^{in}	Intracellular molality of the grouped solute	$\frac{mol}{kg\ water}$
t	Time	min
Parameters that Stay Constant Within a Run		
Symbol	*Description*	*Value/Unit*
L_p^*	Hydraulic conductivity, fitting parameter	$\frac{\mu m}{atm \cdot min}$
P_s^*	DMSO permeability, fitting parameter	$\frac{\mu m}{min}$
L_p^{RT}	Reference value of L_p at room temperature	$\frac{\mu m}{atm \cdot min}$
P_s^{RT}	Reference value of P_s at room temperature	$\frac{\mu m}{min}$
E_{aL_p}	Activation energy of L_p temperature dependence	$\frac{kcal}{mol}$
E_{aP_s}	Activation energy of P_s temperature dependence	$\frac{kcal}{mol}$

Table 2 continued.

Parameters that Stay Constant Within a Run		
Symbol	*Description*	*Value/Unit*
R	Gas constant[41]	$82.06 \times 10^{12} \frac{\mu m^3 \cdot atm}{K \cdot mol}$
T	Temperature, measured (when it stays constant, as in room temperature runs)	K
T_{RT}	Room temperature, measured	K
ρ_w	Density of water, calculated with temperature dependence (when it stays constant, as in the low temperature runs) using Equation (20)[39]	$\frac{kg}{\mu m^3}$
ρ_p	Density of DMSO, calculated with temperature dependence (when it stays constant, as in the low temperature runs) using Equation (21)[40]	$\frac{kg}{\mu m^3}$
π^{ex}	Extracellular osmolality, CPA: calculated with Equation (13), CPA-free: measured	$\frac{Osm}{kg\ water}$
a_p^{ex}	Extracellular activity of DMSO	
V_0	Total volume of the cell at isotonic conditions	μm^3
b^*	Osmotically inactive fraction, fitting parameter	
B_{pp}	Second osmotic virial coefficient of DMSO[28]	$0.108 \frac{kg\ water}{mol}$
C_{ppp}	Third osmotic virial coefficient of DMSO[28]	$0 \left(\frac{kg\ water}{mol}\right)^2$
B_{gg}	Second osmotic virial coefficient of the grouped solute, fitting parameter	$\frac{kg\ water}{mol}$
C_{ggg}	Third osmotic virial coefficient of the grouped solute, fitting parameter	$\left(\frac{kg\ water}{mol}\right)^2$
B_{NN}	Second osmotic virial coefficient of NaCl[28]	$0.044 \frac{kg\ water}{mol}$
C_{NNN}	Third osmotic virial coefficient of NaCl[28]	$0 \left(\frac{kg\ water}{mol}\right)^2$
m_p^{ex}	Extracellular molality of DMSO, measured	$\frac{mol}{kg\ water}$
m_N^{ex}	Extracellular molality of NaCl	$\frac{mol}{kg\ water}$
k_N	Dissociation constant of NaCl[28]	1.678
M_w	Molar mass of water[42]	$0.01802 \frac{kg}{mol}$

Table 2 continued.

Parameters that Stay Constant Within a Run		
Symbol	*Description*	*Value/Unit*
M_p	Molar mass of DMSO[43]	$0.078133\ \frac{kg}{mol}$
N_g^0	Intracellular number of moles of the grouped solute at isotonic conditions	mol
m_g^0	Intracellular molality of the grouped solute at isotonic conditions	$\frac{kg\ water}{mol}$
π^0	Isotonic osmolality, measured	$\frac{Osm}{kg\ water}$

1.3. Scope of this Thesis

In this work, I build on the previously mentioned studies by developing a novel method to fit for the permeability parameters, L_p^* and P_s^*, and their temperature dependence, the osmotically inactive fraction, b^*, and the second and third osmotic virial coefficients for the intracellular grouped solute, B_{gg} and C_{ggg}, respectively. As Zielinksi et al. showed, b^* is more sensitive than B_{gg} to non-permeating solute cell volume data, while B_{gg} and C_{ggg} are more sensitive to permeating solute cell volume data. Therefore, L_p^* and b^* are fit to non-permeating solute cell volume data, and P_s^*, B_{gg}, and C_{ggg} are fit to permeating solute, or CPA-containing, cell volume data iteratively. Thus, starting with the ideal, dilute assumption (B_{gg} = C_{ggg} = 0), L_p^* and b^* are found by fitting the model to kinetic non-permeating solute cell volume data, and these values are used to obtain P_s^*, B_{gg}, and C_{ggg} by fitting the model to kinetic CPA cell volume data. These values for B_{gg} and C_{ggg} are then used to find a new L_p^* and b^*, and this process continues until the parameters converge. This iterative fitting process is described in more detail in Section 2.2.2. Subsequently, the temperature dependence of L_p^* and P_s^* are investigated by fitting CPA-free and

CPA data at a different temperature to the activation energies E_{aL_p} and E_{aP_s}, respectively. The equations from Zielinksi et al. that were used for the fittings are explained in Section 1.2. This novel fitting procedure is conducted for HUVEC and H9C2 cardiomyocyte data collected for this work, which resulted in obtaining five cell-specific parameters and the temperature dependence of the permeability parameters for each cell type that are required to model the changing cell volume during cryopreservation under the assumption that the intra- and extracellular solutions are not ideal. A schematic diagram of the transport between the intra- and extracellular space is illustrated in Figure 1.

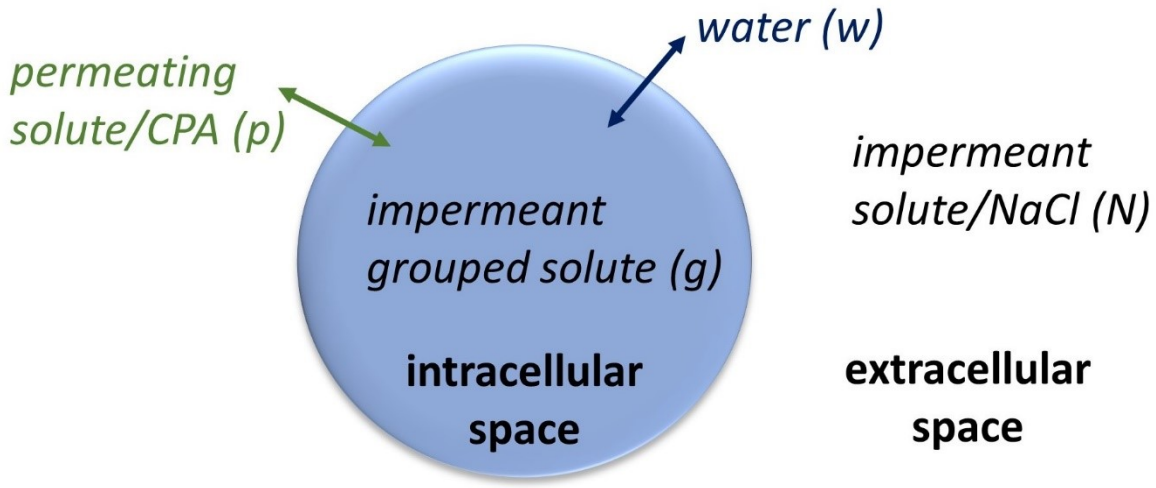

Figure 1. Schematic diagram of transport across cell membrane.

Chapter 2. Methodology

The five cell-specific parameters required for the modelling of the changing cell volume during cryopreservation are L_p^*, b^*, B_{gg}, C_{ggg}, and P_s^*. In this work, these parameters are obtained for human umbilical vein endothelial cells (HUVECs) and rat cardiac muscle cells (H9C2) by conducting two different kinetic cell volume experiments, where the cells are exposed to a hypertonic extracellular environment in the presence and absence of a cryoprotective agent (CPA), specifically dimethyl sulfoxide (DMSO), at room temperature. The CPA-free data are fitted with the equations summarized in Table 2 to obtain L_p^* and b^*, while the CPA data are fitted with the equations in Table 2 to obtain B_{gg}, C_{ggg}, and P_s^*. The parameters L_p^*, b^*, B_{gg}, and C_{ggg} are required in both the CPA and CPA-free fittings, thus an iterative process is conducted by using L_p^* and b^* obtained from the CPA-free data to fit for B_{gg}, C_{ggg}, and P_s^* to the CPA data, and refitting for L_p^* and b^* using the new B_{gg} and C_{ggg} for the CPA-free data. The iterations are continued until the parameters remain the same after an iteration. Additionally, the temperature dependence of L_p^* and P_s^* are obtained by fitting the same equations and the Arrhenius equations to CPA-free and CPA experimental data, respectively, at a different temperature using the B_{gg} and C_{ggg} obtained from the new fitting procedure at room temperature. After the final five cell-specific parameters and the temperature dependence of L_p^* and P_s^* are obtained, these parameters can be used to model the changing cell volume during the entire cryopreservation process.

2.1. Experimental Methods

2.1.1. Cell Cultures

Human umbilical vein endothelial cells (HUVECs) (Lonza, Walkersville, MD, USA) (lot number: 0000486264) were cultured in an incubator at 37 °C and 5% CO_2 in 75 cm^2 flasks with Endothelial Basal Medium-2 (EBM-2) (Lonza, Walkersville, MD, USA) that was previously mixed with Endothelial Cell Growth Medium-2 Bulletkit (EGM-2) (Lonza, Walkersville, MD, USA), which includes fetal bovine serum (FBS), hydrocortisone, ascorbic acid, vascular endothelial growth factor (VEGF), human fibroblast growth factor B (hFGF-B), R3 insulin-like growth factor (R3-IGF-1), and human endothelial growth factor (hEGF). The antibiotic that is included in the EGM-2 BulletKit was not added to the mixture. At 70 to 90% confluency, the cells were passaged with 0.025% trypsin/0.01% EDTA (Lonza, Walkersville, MD, USA) for 2 to 3 minutes in the incubator, neutralized with trypsin neutralizing serum (TNS) (Lonza, Walkersville, MD, USA), and mixed with HEPES buffered saline solution (Lonza, Walkersville, MD, USA). The cell passaging was conducted in a biosafety cabinet. The cells in suspension were placed in 50 mL tubes and centrifuged at 1000 rpm (140 g) for 5 minutes at room temperature in an Eppendorf 5810R tabletop centrifuge (Eppendorf AG, Hamburg, Germany). If an uneven number of tubes were available to centrifuge, an additional tube filled with the same volume of distilled water was used to balance the weight placed in the centrifuge. After separating the supernatant from the cells, 1 to 2 mL of the EBM-2 and EGM-2 mixture was added per flask, depending on the percentage of confluency.

Rat cardiac muscle cells (H9C2) (ATCC, Manassas, VA, USA) (lot number: 70026606) were also cultured in an incubator at 37 °C and 5% CO_2 in 75 cm^2 flasks with ATCC-formulated Dulbecco's Modified Eagle Medium mixed with 10% fetal bovine serum (FBS) (Gibco, Life

Technologies, Grand Island, NY, USA). These cells were passaged when 50 to 70% confluency was reached using 0.25% trypsin/0.53 mM EDTA with phenol red (Gibco, Life Technologies, Grand Island, NY, USA). The cells were passaged in a biosafety cabinet, and the cells in suspension were centrifuged using the same Eppendorf centrifuge at the same conditions described above.

Both cell types were counted with a Coulter® Z_2™ particle count and size analyzer (Beckman Coulter, Mississauga, ON, Canada) or with a hemocytometer. These two cell-counting methods were conducted for the same sample, and the results of the total cell counts are comparable, where the total cell count per mL was 800,324 and 772,500 when using the Coulter® counter and the hemocytometer, respectively. If further experimentation was required, some cells were used to culture again. The remaining cells were used in experimentation. If the experiments were to begin longer than one hour after the passaging was completed, these cells suspended in the media mixture were set in ice to avoid cell clumping.

2.1.2. Solution Preparation

A stock solution of ten times phosphate buffered saline (10x PBS), specifically 10x Dulbecco's Phosphate Buffered Saline (Gibco, Life Technologies, Grand Island, NY, USA), was diluted with deionized water to create the desired osmolalities of PBS. The osmolality of the 10x PBS solution is around 3000 mOsm/kg. The experimental solutions were prepared by measuring the volume of the stock solution and adding the required volume of water to dilute it by the desired factor. The osmolalities of the prepared solutions were measured using a Micro-Osmette Model 5004 freezing point depression osmometer (Precision Systems, Inc., Natick, MA, USA). If some of the prepared solution was left over for the next day of experimentation, the osmolality was

remeasured on the next day. The stock solution was diluted ten times to create the desired solution of 1x PBS to use for the measurement of the isotonic volume of the cells, which was 274.8 ± 2.7 mOsm/kg. Solutions of 2x, 5x, 6x, and 9x PBS were used to measure the changing cell volume of HUVECs for the experimental runs without any cryoprotecting agents. For the H9C2 cells, only 5x PBS was used to measure the changing cell volume, and 1x PBS was used to measure the isotonic cell volume.

For the experimental runs with a cryoprotective agent, solutions of varying molalities of dimethyl sulfoxide (DMSO) (Fisher Scientific, Nepean, ON, Canada and Sigma-Aldrich, Oakville, ON, Canada) were used with the HUVECs, specifically solutions of 1, 2, and 3 molal DMSO, and only 3 molal DMSO was used with the H9C2 cells. The solvent used was a solution of 1x PBS, which was prepared as described above. The 1x PBS solution and the required amount of DMSO were weighed using a Mettler Toledo PG603-S analytical balance (Mettler Toledo, Missisauga, ON, Canada) and mixed. The DMSO obtained from Fisher Scientific appeared to have small white fibers in the solution, so the mixed solution was filtered using a 0.22 micron pore size 500 mL Steritop-GP Threaded Bottle-Top Filter (MilliporeSigma, Burlington, MA, USA) to remove these fibers because fibers in the solution would interrupt the measurements of cell volumes during the experimental run. The reason for these fibers is unknown, as the DMSO obtained from Sigma-Aldrich did not appear to have fibers, and the bottles were stored in the same cabinet at room temperature. The experimental runs using the second bottle of DMSO that did not require filtration are noted with a dagger symbol (†) in the results for the separate fittings of all runs in the Appendix. All other DMSO runs used the first bottle that did require filtration. All components and the mixing process were kept at room temperature, thus crystallization or solidification of the DMSO would

be unexpected. The proper safety precautions were taken when handling DMSO. To reduce the time that the cells spend in suspension, the solutions are prepared before passaging the cells.

2.1.3. Coulter® Counter Z_{B1}™

The Coulter® Z_{B1}™ counter (Beckman Coulter, Mississauga, ON, Canada), fitted with a microcomputer interface created by Dr. Locksley McGann,[44] measures the dynamic volume of the cells by recording a peak value and timestamp of each passing cell. The peak value is a measure of the displacement in potential across the aperture when the cells pass through this aperture. A diagram of the Coulter® counter is illustrated in Figure 2. For the isotonic cell volume experiments, 10 mL of the 1x PBS solution were added into 20 mL blood dilution vials (VWR International, Edmonton, AB, Canada) and 250×10^3 cells are subsequently added to the vial, resulting in a cell concentration of around 25×10^3 cells per mL. The cell concentration must be high enough to capture the rapid shrinking or swelling of the cells, but low enough to reduce the risk of clogging the aperture and remain below the maximum cell density at which coincidence is negligible as specified in the Coulter® counter manual, which is 30×10^3 cells per mL. The mixing magnet is added to the vial, and the vial is placed on a RT Basic Series Stirrer (Thermo Fisher Scientific, Burlington, ON, Canada) with the tube of the Coulter counter submerged in the solution. Then, the stirrer or mixer is turned on, the Coulter® counter is started, and the Cell Size Analyzer (CSA) Data Acquisition program is set to record the measured peaks and their corresponding timestamps. The experiment is run for about 30 seconds. After the run, the program is stopped, the valve on the counter is closed, and the mixer is turned off.

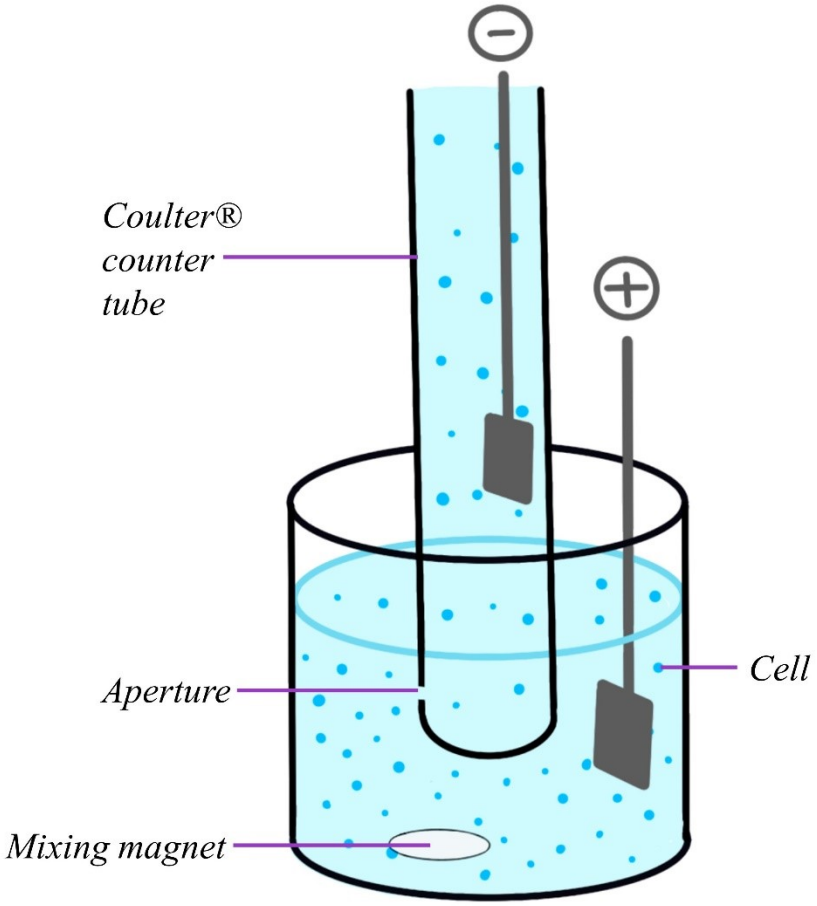

Figure 2. Diagram of Coulter® counter tube and cells in vial.

For the changing cell volume experimental runs, the starting process must be changed because a vital part of the data is gathered at the start of the run when the cells shrink or swell. Thus, the cells must be added after the program is running and the valve is opened. When the cells are added to the vial containing just PBS at higher than 1x concentration, the cells will shrink, as the extracellular environment in the vial has a higher osmolality. When the cells are added to the vial containing 1x PBS and DMSO, the cells initially shrink because of the exposure to an extracellular environment with a higher osmolality, and then swell back up as the DMSO enters the cell and equilibrates the intra- and extracellular environment. Both the CPA and CPA-free experimental runs are continued until equilibrium was reached, except for the CPA runs at 4 °C. While the experiment is running, the level of the solution in the vials lowers as the solution goes

through the aperture and into the tube, which only allows for a maximum run time of about 4 minutes when using the maximum solution volume of 18 mL. We found that the time it takes for both cell types to reach equilibrium during the CPA runs at 4 °C is longer than these 4 minutes. Therefore, these runs were only used to obtain P_s^*, which is affected by the initial shrinking and swelling part of the runs, not the equilibrium. The method of addition of the cells to the vial while the experiment is running is crucial to the quality of the data. Because the shrinking or swelling occurs immediately as the cells come in contact with the solution in the vial, the addition of cells should be done quickly and close to the aperture of the counter's tube.

It is important to note that all calibration runs were conducted three times on each day of experimentation for all osmolalities of PBS and molalities of DMSO that were used on that day. Additionally, the isotonic volume runs were conducted three times each day of experimentation, because it was concluded that the mean isotonic cell volume differed slightly on different days of experiments. Lastly, the changing cell volume experimental runs were conducted three times for each osmolality of PBS and molality of DMSO on each day of experimentation, unless noted otherwise.

The peak measured in the counter is an arbitrary factor between 0 and 255 that depends on the settings chosen on the counter. Settings that are available to be adjusted are the amplification, the aperture current, the lower and upper thresholds, the matching switch, the gain trim, and the aperture size. The settings were chosen based on capturing the greatest number of peaks measured in an isotonic environment run in the middle of the range. The amplification and aperture current were set to 8 and 1, respectively, for both the HUVECs and H9C2 cells. The thresholds were left at the minimum and maximum. The maximum switch was set to 20×10^3, and an aperture size of 100 μm in diameter was chosen for both cell types. The gain trim was set to 9 and 2 for the

HUVECs and H9C2 cells, respectively. To calibrate these settings with the measured peak values, 10 and 15 μm diameter latex beads (Beckman Coulter, Mississauga, ON, Canada) were used for the HUVECs. These two sizes of beads were used because the diameter of HUVECs is most comparable to them, as opposed to 5 or 20 μm beads. For the H9C2 cells, the 15 μm beads were used. These calibration runs allow for the calculation of a calibration factor, f, using the following equation

$$f = \frac{V_{beads}}{p}, \tag{22}$$

where V_{beads} is the volume of the beads and p is the average peak measured during the calibration run. This is later used to convert the measured peaks in the isotonic volume and changing volume runs to a size in terms of volume. To further minimize the amount of time the cells spend in suspension after trypsinization, the calibration runs with latex beads were conducted before preparing the cells.

Some safety concerns to consider when working with this Coulter® counter are that the waste container must not overflow, the light bulb that allows the viewing of the aperture becomes very hot, which can burn the operator's hand when handling the vial or tube, and there is a mercury-filled tube in the pressure mechanism of the counter, which can pose severe health effects if exposed to the operator.

2.1.4. Method Developments

The last time the Coulter® counter was used in the Elliott/McGann lab group was about 10 years before this work. Before starting experimentation, a lot of dust had to be cleared and techniques and tricks had to be learned and perfected. The cell concentration was optimized to

ensure that the cell size distribution was well represented, while also not clogging the aperture and having enough cells to complete the desired runs. This also depended on the aperture size, where if too small, it would clog, but if too big, the differentiation in the deviation of electric potential would be difficult to capture. The cell concentrations tested were 10×10^3, 25×10^3, 30×10^3, 50×10^3 cells per mL solution. The concentrations with a smooth enough cell size distribution and smaller chance of clogging were 25×10^3 and 30×10^3, so to ensure enough cells were available on each day of experimentation, 25×10^3 was the final choice. The aperture sizes 50, 70, 100, and 140 μm were tested. To be able to capture most of the cell size distribution and avoid clogs, 100 μm was chosen for the HUVECs and H9C2 cells. The diameter calculated from the measured isotonic volumes of HUVECs and H9C2 cells are 15.47 ± 0.28 μm and 19.31 ± 0.26 μm, respectively. The parameter settings chosen on the Coulter® counter also depend on the aperture size and the cell size. The parameters were optimized for HUVECs by testing different combinations of the amplitude and gain trim. The amplitude setting is to adjust were the peaks lie in the window on the Coulter® counter. The goal is to have most of the peaks measured during an isotonic volume run reach the middle of the window to capture most of the cell size distribution and ensure the shrinking is also captured when conducting hypertonic cell volume runs. The gain trim is the fine detailing of the amplitude setting. Lastly, analyzing the first few test runs, the number of cells measured per time interval appeared to increase during the run as the level of the solution in the vial decreased. This meant the cells were not mixed in the solution and gathered at the top of the solution, and a small enough mixer that fit in the Coulter® counter was needed.

2.1.5. Temperature Conditions

The kinetic and isotonic volume runs were conducted at room temperature and 4 °C. The temperature of the solution in the vial was measured before and after the run was completed with the Temp300 JTEK Data Logging Thermocouple (Thermo Fisher Scientific, Singapore). For the experiments at 4 °C, the vials containing solution were placed in ice and left to cool down to the desired temperature for over 2 hours. The temperature of the solution in the vials was measured before and after each run at 4 °C, and the temperature was assumed to increase linearly with time from the initial to the final temperature measured. Additionally, the remaining solution that was to be used to flush the Coulter® counter was placed in a refrigerator at 4 °C to reduce the temperature increase during the run. For the experiments at room temperature, the vials and the remaining solution used to flush the Coulter® counter were left at room temperature on the laboratory bench. At room temperature, the temperature of the solution in the vials was only measured for the H9C2 cells. The overall average temperature of the CPA-free runs at room temperature measured for the H9C2 cells was used for the CPA-free runs for the HUVECs, and the average temperature of the CPA runs at room temperature measured for the H9C2 cells was used for the CPA runs for the HUVECs. The difference in temperature between the CPA-free and CPA runs comes from the slight increase in temperature when mixing DMSO with the 1x PBS solution.

2.2. Data Analysis Method

2.2.1. Cell Size Analyzer (CSA) Program

The files that were created when recording the peaks measured by the Coulter® counter were opened and analyzed with the Cell Size Analyzer (CSA) program created by Dr. Locksley McGann. When opening a file on the program, three other windows open. The “Histogram”, “Raw

Data", and "Mean vs Time" windows illustrate the frequency or number of points of the peak values in the run, the raw data file with all measured points versus time, and the mean peak value per time interval versus time, respectively. The original window for the program and the three windows that open once a file is selected are illustrated in Figure 3, Figure 4, Figure 5, and Figure 6, with a sample run of 5x PBS. The start and end times of the run were adjusted by dragging the vertical red lines in the "Raw Data" window to the section of time that is to be excluded, checking data "Invalid", and clicking on "Apply". This would remove the squared off section of data from the run. Additionally, the lower and upper thresholds were adjusted in the program, which are denoted with the horizontal red lines in the "Raw Data" window and the vertical red lines in the "Histogram" window. For the isotonic and experimental runs, the thresholds were adjusted by choosing the minimum frequency or number of peaks as illustrated in the "Histogram" window. There is also a smoothing option in the "Histogram" window, but this option was never modified. Lastly, the time interval for the average peak values can be adjusted, which can result in the average data points being less scattered. However, there was no correlation between increasing or decreasing the time interval and an increase or decrease in the scattering of the data, so this interval was frequently left at the programmed value of 500 ms.

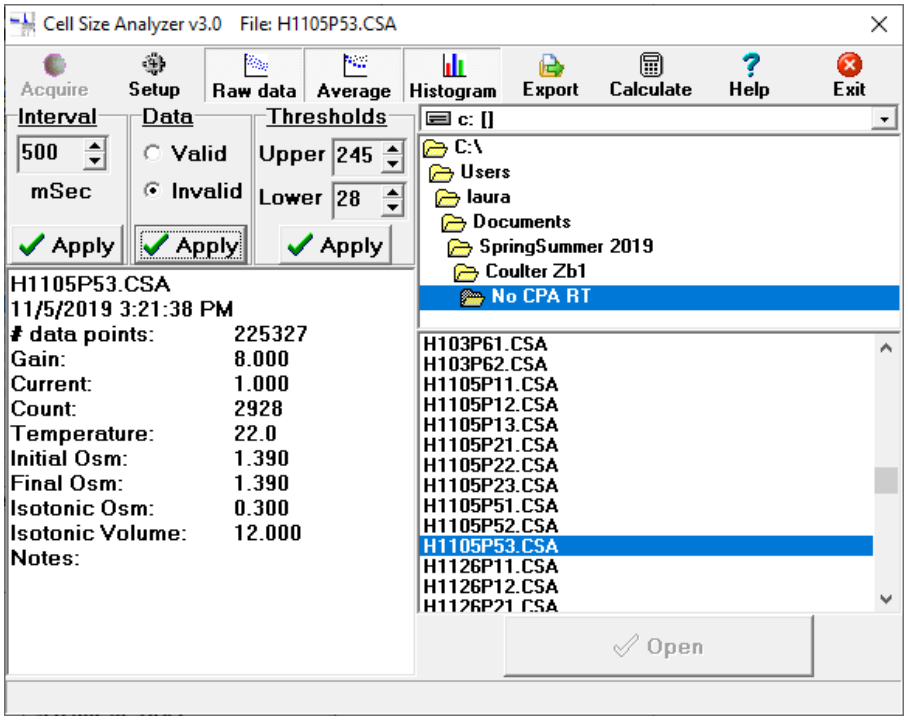

Figure 3. Original window from the Cell Size Analyzer program.

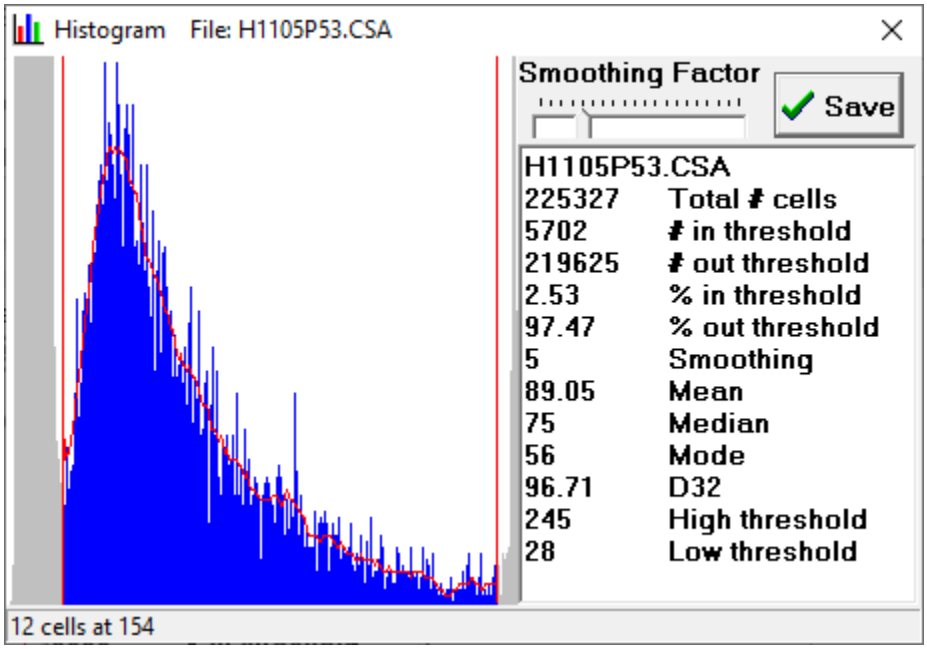

Figure 4. Histogram window from the Cell Size Analyzer program displaying number of cells measured at varying peak heights and additional information about the total number of cells, the cells within the current threshold, and the average types for the current threshold.

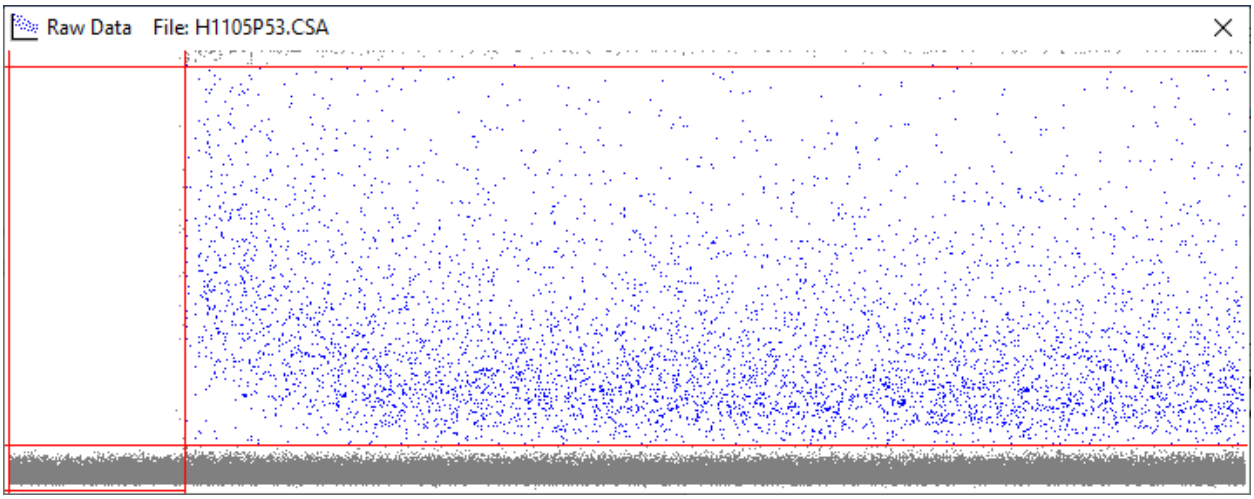

Figure 5. Raw Data window from the Cell Size Analyzer program displaying all data points obtained in terms of peak versus time. The vertical red lines are used to exclude the timespan of data where there are no peaks or the aperture was clogged, which would appear as a disruption in the mean cell volume.

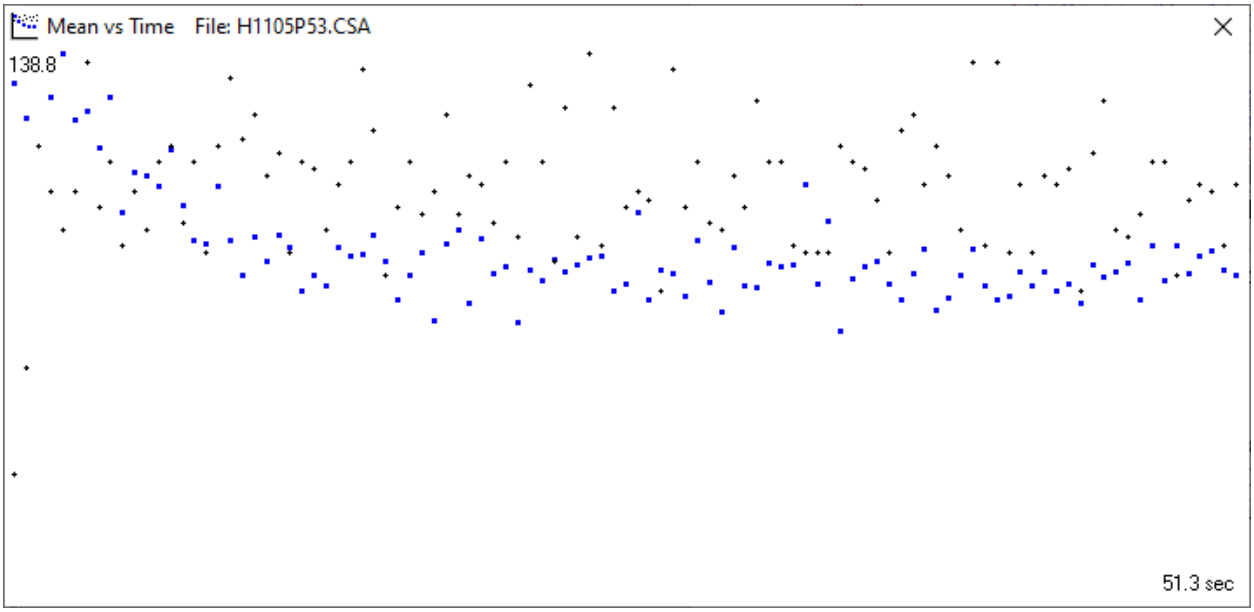

Figure 6. Mean vs Time window from the Cell Size Analyzer program displaying the mean peak measured within the time interval (chosen in the Original window) in blue dots and the total number of points per time interval in black dots.

The program also allows the average type to be chosen from mean, mode, median, and D32 by clicking on “Calculate” in the original window. A study found that for lognormal distributions, which is the distribution seen for the cell volume of cells that are growing and dividing such as

HUVECs or H9C2 cells, either the mean or median would be the best average type to represent the cell volume distribution.[45] In the current work, the mean cell volume was used to describe the average cell volume, which is calculated as the sum of all peak heights in each time interval divided by the total number of peaks in that time interval.

The calibration runs with latex beads and the isotonic volume runs require the adjustment of the aforementioned settings in the program, and the text that appears in the "Histogram" window was used. The mean peak value that is shown in this window describes the mean of all measured points in the selected timespan. The mean value of the calibration run is used to calculate the calibration factor as described in Equation 22. Subsequently, the mean value of the isotonic volume runs is used to calculate the mean isotonic volume with the calibration factor. The CPA and CPA-free experimental runs are obtained by adjusting these settings and clicking on "Export" in the original window then "Mean vs Time", which creates a text file of a table with the same information in the "Histogram" window and the time, number of peaks per time interval, and the mean peak value of that time interval in three columns. The tables created were inserted into Excel and columns were added to convert the peak values into volume using the calibration factor. Lastly, the volume of the cell is converted into the relative volume by dividing by the measured isotonic volume of the corresponding day of experiments.

2.2.2. Fitting Data to the Theoretical Model in MATLAB

After obtaining the time versus relative volume table, the data was input into MATLAB and a program solved for the desired parameters. A program was written to solve for L_p^* and b^* by fitting the CPA-free data to Equation 1, and another program was written to solve for P_s^*, B_{gg}, and

C_{ggg} by fitting the CPA data to Equations 1 and 2. Both programs utilize the built-in function 'lsqcurvefit' from MATLAB, which solves non-linear problems using least squared errors, meaning it minimizes the sum of the squares of residuals of the fit to the experimental data by changing the values of L_p^* and b^*, and P_s^*, B_{gg}, and C_{ggg} in the fittings to the CPA-free and CPA experimental data, respectively. For the CPA-free data, changing L_p^* results in the initial decrease (for hypertonic extracellular solutions) in volume being steeper or more gradual, and changing b^* affects equilibrium volume. Thus, changing these two parameters at the same time would have no impact on each other. For the CPA data, adjusting P_s^* affects the minimum point (for hypertonic extracellular solutions), and changing B_{gg} and C_{ggg} result in changes in the equilibrium volume.

The CPA-free fitting only requires the solution of one ordinary differential equation (ODE), and a non-stiff ODE built-in function in MATLAB, specifically 'ode45', was used. Stiff ODE solvers are used when the solution of the ODE varies in magnitude in the desired range. Non-stiff ODE solvers are recommended to use, because they are more accurate, but they require longer computation times.[46,47] For this simple ODE solution in the CPA-free model, 'ode45' works well with a short computation time. For the CPA data, the computation time is expected to be longer, because the solution includes a system of ODEs and more complicated computations. Therefore, a stiff ODE solver was initially used for this fitting, but the solution was highly dependent on the initial guesses chosen for P_s^*, B_{gg}, and C_{ggg}. For example, choosing 5 versus 10 as an initial guess for B_{gg} results in a different answer for B_{gg}. By changing the ODE solver to 'ode45' and choosing initial guesses for P_s^*, B_{gg}, and C_{ggg} that are relatively close to the expected magnitude, the solution is more accurate and not dependent on the initial guesses chosen. This requires a longer computation time of about a couple of minutes, which is acceptable for the purposes of this work.

Before finding the five parameters for each cell type, the time gap between the time of addition (t_0) and the time when the first few cells passed through the aperture (t_1) was adjusted for each run at room temperature. To achieve this, a 'for loop' was added to the MATLAB codes for the CPA-free and CPA runs that aims to minimize the sum of squared errors by adjusting the gap between t_0 and t_1. The equation used for the sum of squared errors is as follows

$$Error = \sum \left(\frac{V_{cell}}{V_0} - \frac{V_{data}}{V_0} \right)^2 , \tag{23}$$

where $\frac{V_{cell}}{V_0}$ is the relative theoretical cell volume and $\frac{V_{data}}{V_0}$ is the relative experimental cell volume at each time data point. The loop creates the time data points column by adjusting t_1 in each loop. The time column is further generated by using the same time interval used in the experimental run and the total length of the time column is equal to the number of data points from the run. The loop is continued until the threshold set for the error in Equation 23 is reached. To find the minimum error, the threshold is manually decreased until the final calculated error is above the threshold. In other words, if the error threshold is set to 0.5, but the final error calculated by MATLAB is above 0.5, then the loop did not converge, and the threshold must be increased to the previous successful value. The error threshold is manually decreased until this final calculated error is above the threshold, and the previous threshold is used as the minimum. For the 5x PBS runs at room temperature, B_{gg} and C_{ggg} are set equal to 0 when finding the time gap. The average L_p^* and b^* found during these time gap fittings are used to find the time gaps for the 3 molal DMSO runs at room temperature.

After the time gaps for all runs at room temperature are obtained, the 5x PBS runs at room temperature with their new time columns are combined and the same is done for the 3 molal DMSO

runs at room temperature. These are used for the fitting procedure to obtain all five parameters. Figure 7 illustrates a flowchart for the fitting process, which is described in detail below. First, the CPA-free data is fitted to find L_p^* and b^* with B_{gg} and C_{ggg} equal to 0. Next, the L_p^* and b^* found in the first step are used to fit the CPA data to find P_s^*, B_{gg}, and C_{ggg}. With these values for B_{gg} and C_{ggg}, the CPA-free data is refit for L_p^* and b^*. If the values for L_p^* and b^* have not changed, the iterations are stopped, but if they have changed, then these values are used to refit the CPA data for P_s^*, B_{gg}, and C_{ggg}. This process is continued until the parameters remain the same after an iteration. The osmolality chosen to represent the CPA-free data in this new fitting method was 5x PBS because this was the osmolality that had more sample runs for HUVECs. The molality chosen to represent the CPA data was 3 molal DMSO because the parameters P_s^*, B_{gg}, and C_{ggg} are expected to be more sensitive in higher concentrations of cryoprotectants. After the five parameters have been found, the 5x PBS runs are fit separately using B_{gg} and C_{ggg} found in the fitting process to find a range for L_p^* and b^*. Similarly, L_p^*, b^*, B_{gg}, and C_{ggg} found in the fitting process are used to find a range for P_s^* by fitting the 3 molal DMSO runs separately. Lastly, runs are separately fit for the time gap again to confirm it has not changed by including the corresponding parameters found in the fitting process in the MATLAB codes, instead of setting B_{gg} and C_{ggg} equal to 0.

For the runs at 4 °C, L_p^* and P_s^* obtained from the fitting method at room temperature are used as the reference point parameters L_p^{*RT} and P_s^{*RT} in Equation 3 and Equation 4, respectively. The values obtained for B_{gg} and C_{ggg} from the fitting method are used for the fittings at 4 °C because they are assumed to be temperature independent. The codes were adapted to include a linear change in temperature over time and the permeability parameters were calculated using the

Arrhenius equation as shown in Equations 3 and 4. The activation energy was chosen as the fitting parameter instead of L_p^* and P_s^* to incorporate the temperature dependence of the fitting parameters. The CPA-free runs at 4 °C were fit to E_{aL_p} and b^*, and the CPA runs at 4 °C were fit to E_{aP_s} using E_{aL_p} and b^* from the CPA-free runs. Before conducting the final fittings for these parameters, the time gaps for all runs at 4 °C were obtained with the adapted codes for changes in temperature.

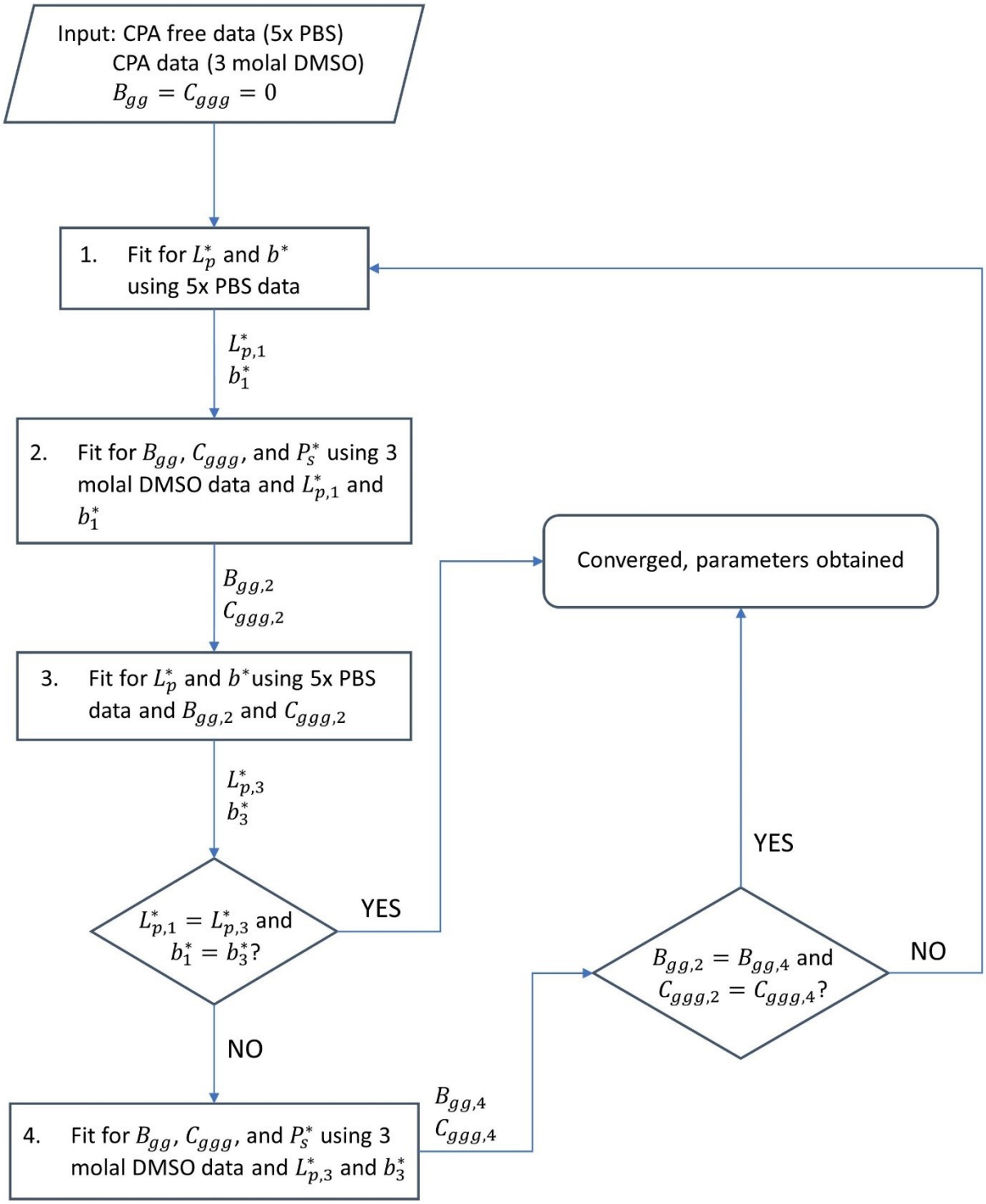

Figure 7. Flowchart of new fitting method to obtain L_p^*, b^*, P_s^*, B_{gg}, and C_{ggg} from changing cell volume data with and without cryoprotectant.

Chapter 3. Results

3.1 Results of the New Fitting Method at Room Temperature

As mentioned in Section 2.2.2., the 5x PBS runs at room temperature were combined after obtaining the time gaps for each run separately, and the same was done for the 3 molal DMSO runs at room temperature. The iterative fitting method was conducted, and the five parameters were obtained. Then, the time gaps for each separate run were rechecked using B_{gg} and C_{ggg} from the fitting method. For HUVECs, the time gaps were either the same or varied less than 15% from the initial values, and when repeating the fitting method, the parameters varied less than 10% from the first values, but the updated time gaps and fitting parameters were used as the final result. For H9C2 cells, the time gaps varied more than those for HUVECs, and the fitting parameters changed more drastically, and the final parameters with the updated the time gaps were also used. Figure 8 and Figure 9 illustrate the combined 5x PBS and 3 molal fittings with the final parameters obtained with the fitting method for HUVECs and H9C2 cells, respectively. The figure descriptions include the number of repetitions that were conducted for each graph that includes combined runs. Generally, each experimental condition was repeated three times, but there are a few exceptions. For example, the 5x PBS runs of HUVECs at room temperature include six repetitions, three of which were conducted on one day and three on another day, meaning they are of different cell passages. All separate runs and their fittings are reported in the Appendix, and the figure descriptions include the run identification (ID) codes with the dates on which the experiments were conducted. The run ID code formatting is HmmddPx# for HUVECs in PBS and HmmddCx# for HUVECs in CPA. The letters ‘mm’ represents the month and ‘dd’ represents the day. The ‘x’ represents the concentration, and the number sign represents the repetition of that day.

For example, H1024P51 is the first run of HUVECs in 5x PBS on October 24th. For H9C2 cells, the H is replaced with a C. All experiments conducted on the same day are of the same cell passage.

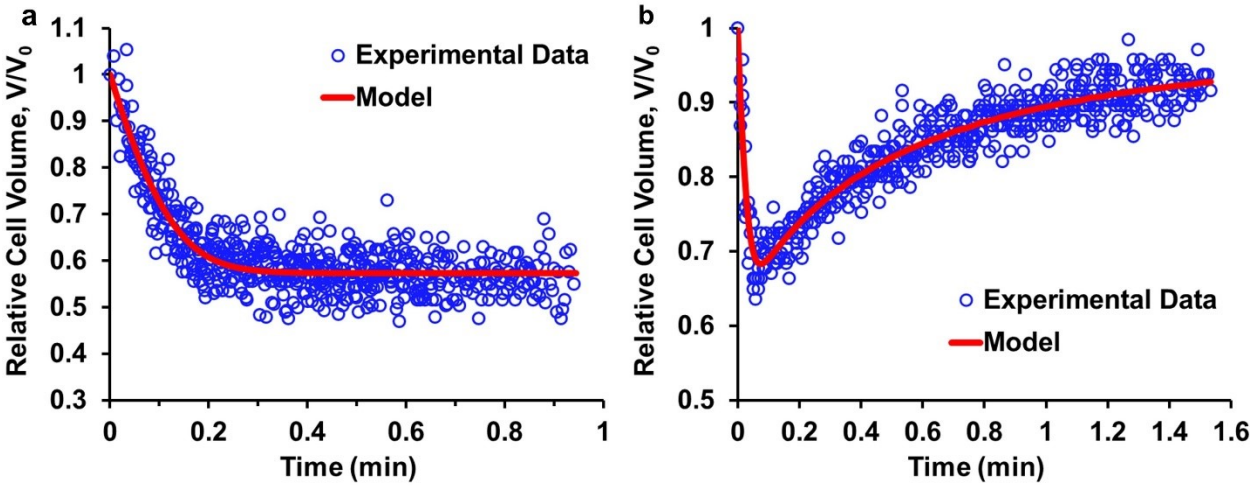

Figure 8. Room temperature experimental data and theoretical model fits for (a) 5x PBS, with n = 6, and (b) 3 molal DMSO, with n = 3, for HUVECs with the final parameters obtained from the new fitting method.

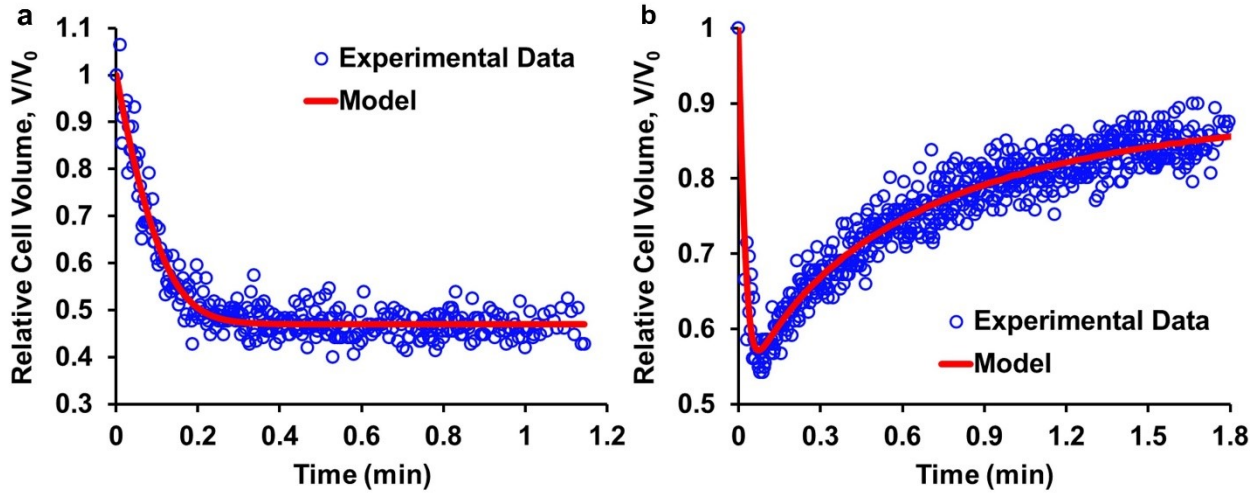

Figure 9. Room temperature experimental data and theoretical model fits for (a) 5x PBS, with n = 3, and (b) 3 molal DMSO, with n = 3, for H9C2 cells with the final parameters obtained from the new fitting method.

The final five parameters for both HUVECS and H9C2 cells are reported in Table 4. The iterative process and the parameters obtained at each step of the iterations for HUVECs and H9C2 cells are reported in Table A1 and Table A2 in the Appendix. It is important to note that when fitting relative volume data to find the parameters L_p^* and P_s^* all variables that include a volume term are calculated using relative volume. The updated equations in terms of relative volume are reported in Table 3. All other equations remain unchanged. This does not affect most parameters, because the relative volumes are canceled out, except for A_{cell}.

Table 3. Updated equations for relative volume fittings.

Equations to model data where a permeating CPA is present	Equation Number
$\frac{d\frac{V_w}{V_0}}{dt} = L_p' A_{cell}(t) RT \rho_w \left[\pi^{in}(t) - \pi^{ex}\right]$	(24) from (1)
$\frac{d\frac{V_p}{V_0}}{dt} = P_s' A_{cell}(t) \left[a_p^{ex} - a_p^{in}(t)\right]$	(25) from (2)
$A_{cell}(t) = 4\pi \left[\frac{3}{4\pi}\frac{V_{cell}(t)}{V_0}\right]^{2/3}$	(26) from (5)
$\frac{V_{cell}(t)}{V_0} = \frac{V_w(t)}{V_0} + \frac{V_p(t)}{V_0} + \frac{b^* V_0}{V_0}$	(27) from (6)
$m_p^{in}(t) = \frac{\frac{V_p(t)}{V_0}\rho_p}{M_p \frac{V_w(t)}{V_0}\rho_W}$	(28) from (16)
$m_g^{in}(t) = \frac{N_g^0}{\frac{V_w(t)}{V_0}\rho_W}$	(29) from (17)
$N_g^0 = m_g^0 \frac{V_0}{V_0}(1 - b^*)\rho_w$	(30) from (18)

Table 3 continued.

Equations to model CPA-free data	Equation Number
$\frac{d\frac{V_w}{V_0}}{dt} = L_p' A_{cell}(t) RT \rho_w \left(\pi^{in}(t) - \pi^{ex}\right)$	(24) from (1)
$A_{cell}(t) = 4\pi \left[\frac{3}{4\pi}\frac{V_{cell}(t)}{V_0}\right]^{2/3}$	(26) from (5)
$\frac{V_{cell}(t)}{V_0} = \frac{V_w(t)}{V_0} + \frac{b^* V_0}{V_0}$	(27) from (6)
$m_g^{in}(t) = \frac{N_g^0}{\frac{V_w(t)}{V_0}\rho_W}$	(29) from (17)
$N_g^0 = m_g^0 \frac{V_0}{V_0}\,(1 - b^*)\rho_w$	(30) from (18)

Therefore, the values for L_p^* and P_s^* reported in Table 4 have been converted using the following equations

$$L_p^* = L_p' V_0^{1/3} \tag{31}$$

and

$$P_s^* = P_s' V_0^{1/3} \tag{32}$$

where L_p' and P_s' are the values obtained for the fittings of L_p^* and P_s^* to the relative volume data using Equations 24 and 25, respectively. The value used for V_0 is the measured value of the isotonic volume on the corresponding day of experimentation for each run. For HUVECs, the combined runs of 5x PBS include runs that were conducted on different days, which have different measured values for V_0, and in this case, the average of these measured values was used. This conversion

factor was confirmed by fitting separate runs to the actual cell volume instead of the relative volume, where the same value was obtained by fitting actual volume data versus fitting relative volume data and using the conversion factor. All experimental runs were fit separately using B_{gg} and C_{ggg} from the fitting method, meaning all CPA-free and CPA runs at room temperature were fit separately for L_p^* and b^* and P_s^*, respectively. The averages and standard deviations for L_p^*, b^*, and P_s^* for HUVECs and H9C2 cells at room temperature are reported in Table 5. It is important to note the possibility of a "loop" convergence when using this method. When this occurs, the parameters do not exactly converge to one value, but will loop between values within a small standard error, thus the parameters can be averaged between the minimum and maximum values of the loop. This is most probably due to the lack of precision in the parameters given from the 'lsqcurvefit' in MATLAB, as these are only reported with four decimals. For example, if the value for L_p' seems to be converging to 0.0267, but more precisely it is 0.02665 being rounded to four decimals, and a next fitting might lead to the rounding of 0.02664, which would be 0.0266 with four decimals, then this could cause the "loop" convergence. This can be avoided by using the longer decimal output in the MATLAB code.

3.2 Results of Experimental Runs at 4 °C

The five parameters obtained from the fitting method at room temperature were used for the fittings at 4 °C. L_p^* and P_s^* values found at room temperature were used as the reference values, L_p^{*RT} and P_s^{*RT}, in the Arrhenius equations. B_{gg} and C_{ggg} were assumed to be temperature independent, thus the same values obtained from the fitting method at room temperature were used for the separate fittings at 4 °C. The temperature was not constant during the experimental runs at

4 °C, so the temperature was assumed to increase linearly between the initial and final temperature measured for each run using the equation

$$T = \left(\frac{T_f - T_i}{t_f - t_0}\right) t + T_i \tag{33}$$

where T_i and T_f are the solution temperatures measured before and after the experimental runs, respectively, and t_0 and t_f are the first and final time points of the experimental run, respectively. In this work, t_0 is always set to 0 and $V(t_0)$ is the isotonic volume V_0, which is equal to 1 in terms of relative volume. It is important to note that when conducting the time gap fittings at 4 °C, t_f must be adjusted continuously because it changes as the time gap changes, and the slope in Equation 33 also changes as a result. The measured values for T_i and T_f are reported in Table A3 in the Appendix.

Initially, b^* was also assumed to be temperature independent, but the values obtained from the separate fittings for H9C2 cells at room temperature were significantly different ($p < 0.05$) from those at 4 °C. For HUVECs, these values were not significantly different, but the fittings were slightly improved with a lower error calculation when including b^* as a fitting parameter at 4 °C. Therefore, the fitting parameters for the CPA-free runs at 4 °C were E_{aL_p} and b^*. These values were then used when fitting for E_{aP_s} to the CPA runs at 4 °C. Example runs of H9C2 cells in 5x PBS and 3 molal DMSO at 4 °C are shown in Figure 10. The averages and standard deviations for E_{aL_p}, b^*, and E_{aP_s} for HUVECs and H9C2 cells at 4 °C are reported in Table 5. All separate fittings for HUVECs and H9C2 cells are illustrated in the Appendix, except for those used as examples in Figure 10.

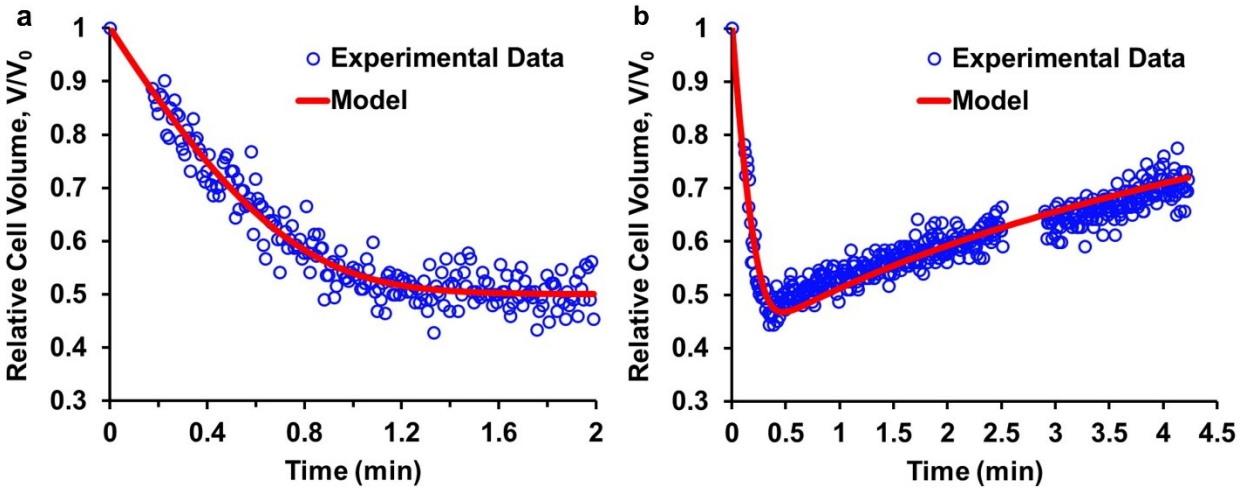

Figure 10. Example runs of H9C2 cells in 5x PBS (run ID: C0811P51) and 3 molal DMSO (run ID: C0917C31) at 4 °C.

Table 4. Five cell-specific parameters obtained with the new fitting method using 5x PBS and 3 molal DMSO for HUVECs and H9C2 cells at room temperature.

Parameter	Unit	HUVECs	H9C2
L_p^{*RT}	$\frac{\mu m}{atm \cdot min}$	0.3434	0.5869
b_{RT}^{*}		0.1801	0.06297
P_s^{*RT}	$\frac{\mu m}{min}$	100.8	133.4
B_{gg}	$\frac{kg\ water}{mol}$	0.4956	0.3772
C_{ggg}	$\left(\frac{kg\ water}{mol}\right)^2$	30.25	8.802

Table 5. Means ± standard deviations of L_p^{*RT}, b_{RT}^*, and P_s^{*RT} from the separate fittings at room temperature, and E_{aL_p}, b_{4C}^*, and E_{aP_s} from the separate fittings at 4 °C for HUVECs and H9C2 cells for 5x PBS and 3 molal DMSO. The parameters b_{RT}^* and b_{4C}^* are the osmotically inactive fraction at room temperature and 4 °C, respectively.

Parameter	Unit	HUVECs	H9C2
L_p^{*RT}	$\frac{\mu m}{atm \cdot min}$	0.347 ± 0.046	0.593 ± 0.061
b_{RT}^*		0.185 ± 0.017	0.0636 ± 0.0245
P_s^{*RT}	$\frac{\mu m}{min}$	101 ± 3	134 ± 15
E_{aL_p}	$\frac{kcal}{mol}$	11.5 ± 0.6	13.6 ± 0.6
b_{4C}^*		0.205 ± 0.060	0.124 ± 0.025
E_{aP_s}	$\frac{kcal}{mol}$	23.7 ± 0.5	21.6 ± 0.8

3.3. Additional Runs for HUVECs at Other Concentrations of PBS and DMSO

Additional runs at varying concentrations of PBS and DMSO were conducted for HUVECs at room temperature, specifically 2x PBS, 6x PBS, 9x PBS, 1 molal DMSO, and 2 molal DMSO. The parameters found using the new fitting method for HUVECs at room temperature, which are reported in Table 4, were used to predict the changing cell volume for all these additional concentrations. The experimental runs for all concentrations were repeated 3 times, except for 2x PBS, which was repeated 4 times. The results for the predicted cell volumes for the runs with 2x PBS, 6x PBS and 9x PBS along with the experimental cell volumes for these runs are illustrated in Figure 11. The results for the predicted cell volume for the runs with 1 molal and 2 molal DMSO along with the experimental cell volumes for these runs are illustrated in Figure 12.

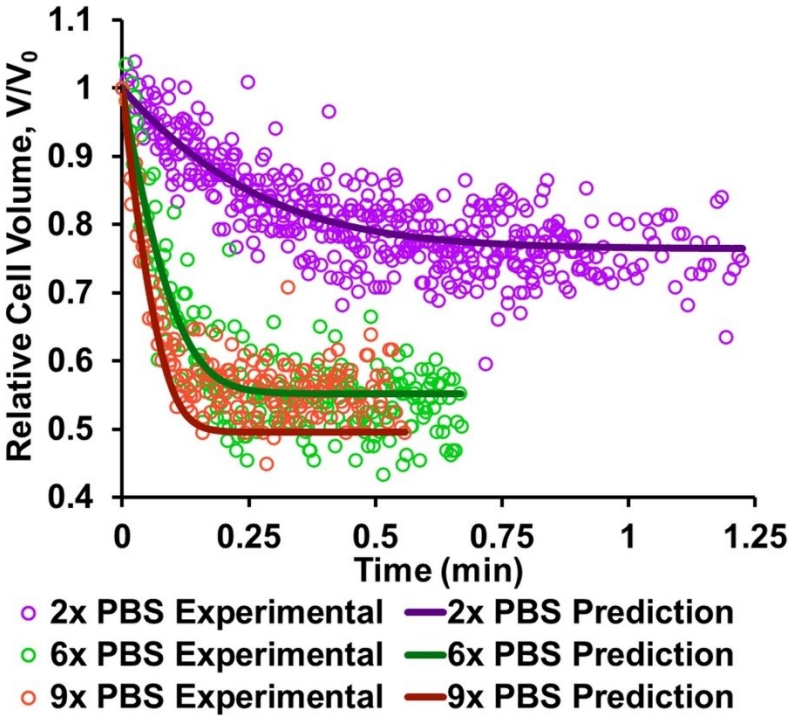

Figure 11. Predicted and experimental cell volumes with 2x PBS (n = 4), 6x PBS (n = 3), and 9x PBS (n = 3) using HUVECs at room temperature.

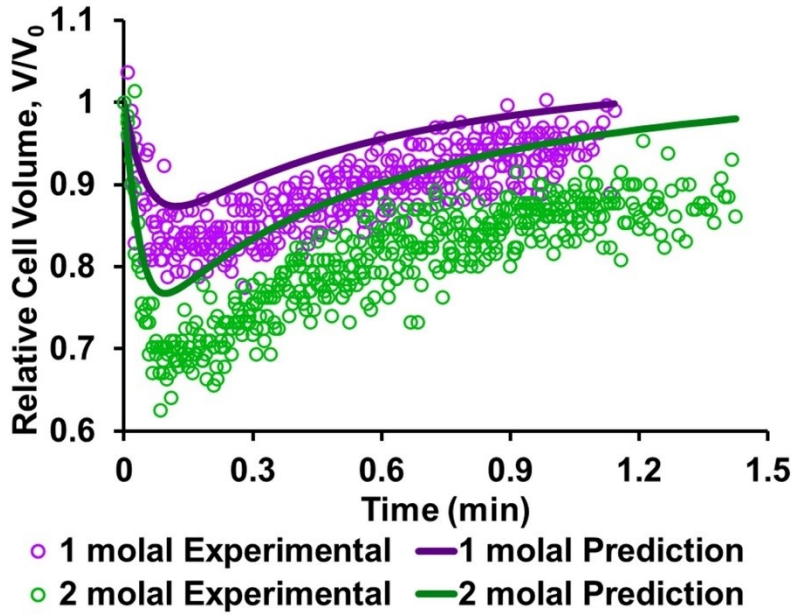

Figure 12. Predicted and experimental cell volumes with 1 molal DMSO (n = 3) and 2 molal DMSO (n = 3) using HUVECs at room temperature.

The cell volume predictions for the different osmolalities of PBS seem to be accurate, especially for 2x PBS and 6x PBS. The equilibrium volume of the 9x PBS runs is slightly underestimated in the predicted cell volume. This might be due to the cells experiencing extreme osmotic damage when placed in the 9x PBS solution, but this is simply a speculation. On the other hand, the predictions for the DMSO runs are not as accurate. For both the 1 molal and 2 molal DMSO predictions, the cell volume is overestimated, specifically when the cells swell back up as DMSO and water are entering the cells. The overestimation is more severe for the 2 molal DMSO runs. The overestimations arise from a value for P_s^{*RT} that is higher than required, so all additional DMSO runs with varying molalities of DMSO, and the 3 molal DMSO runs that were previously separately fit for P_s^{*RT} only, were fit for P_s^{*RT}, B_{gg}, and C_{ggg} using L_p^{*RT} and b_{RT}^* from the fitting method, and all additional PBS runs were fit for L_p^{*RT} and b_{RT}^* using B_{gg} and C_{ggg} from the fitting method to obtain a range of values for these five parameters at varying concentrations and to see how much they vary. The results for the fittings for L_p^{*RT} and b_{RT}^* to the 2x PBS, 6x PBS, and 9x PBS runs are illustrated in Figure 13. The ranges for L_p^{*RT} and b_{RT}^* found by fitting the 5x PBS runs are also included in this figure for comparison purposes.

The results for the fittings for P_s^{*RT}, B_{gg}, and C_{ggg} to the 2 and 3 molal DMSO runs are illustrated in Figure 14. The runs at 3 molal DMSO were refit for P_s^{*RT}, B_{gg}, and C_{ggg} to investigate if adding B_{gg} and C_{ggg} as fitting parameters affects the results for P_s^{*RT}, as the results reported in Table 5 are for fittings to P_s^{*RT} only, and we found no significant difference between the values of P_s^{*RT} when including versus excluding B_{gg} and C_{ggg} as fitting parameters. The results obtained for the fittings of the 1 molal DMSO data were omitted from this figure because the error bars are too off scale, which might be due to the low sensitivity of B_{gg} and C_{ggg} to a low concentration of

DMSO or due to the experimental runs being too short and not adequately representing the equilibrium volume, but the results are numerically reported in Table 6. The height of the bar graphs represents the mean, and the error bar represents the standard deviation of the values obtained for each separate run at each concentration. The results shown in Figure 13 and Figure 14 are summarized in Table 6, and all figures of the separate fittings are reported in the Appendix.

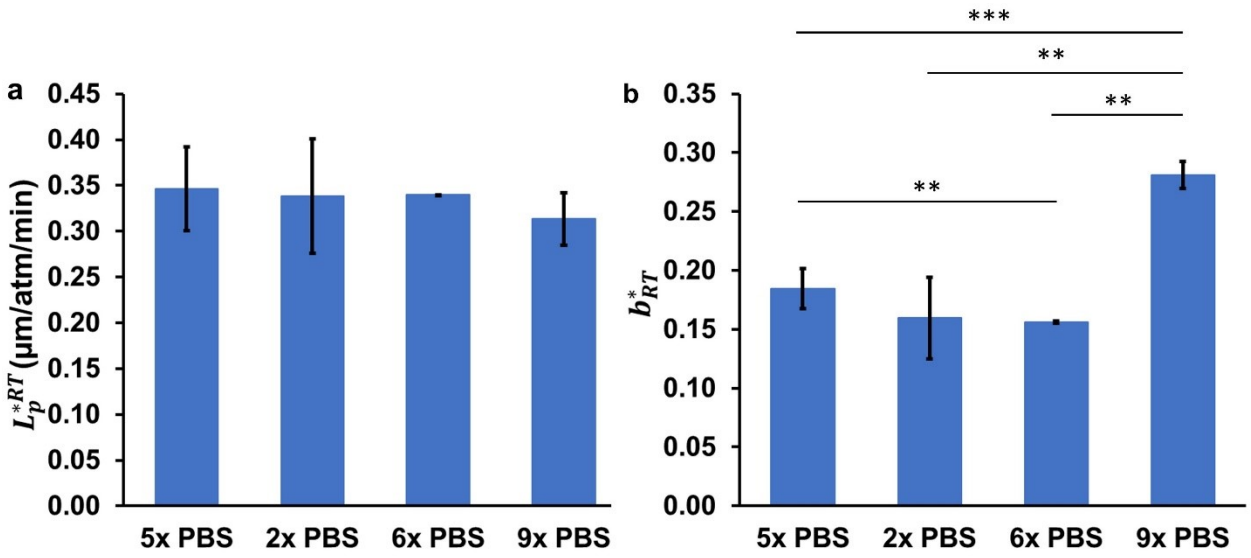

Figure 13. Means and standard deviations of (a) L_p^{*RT} and (b) b_{RT}^* from separate fittings at 5x PBS (for comparison purposes, the same values are reported in Table 4), 2x PBS, 6x PBS, and 9x PBS for HUVECs at room temperature. Significance noted as ** for $p < 0.01$ and *** for $p < 0.0001$.

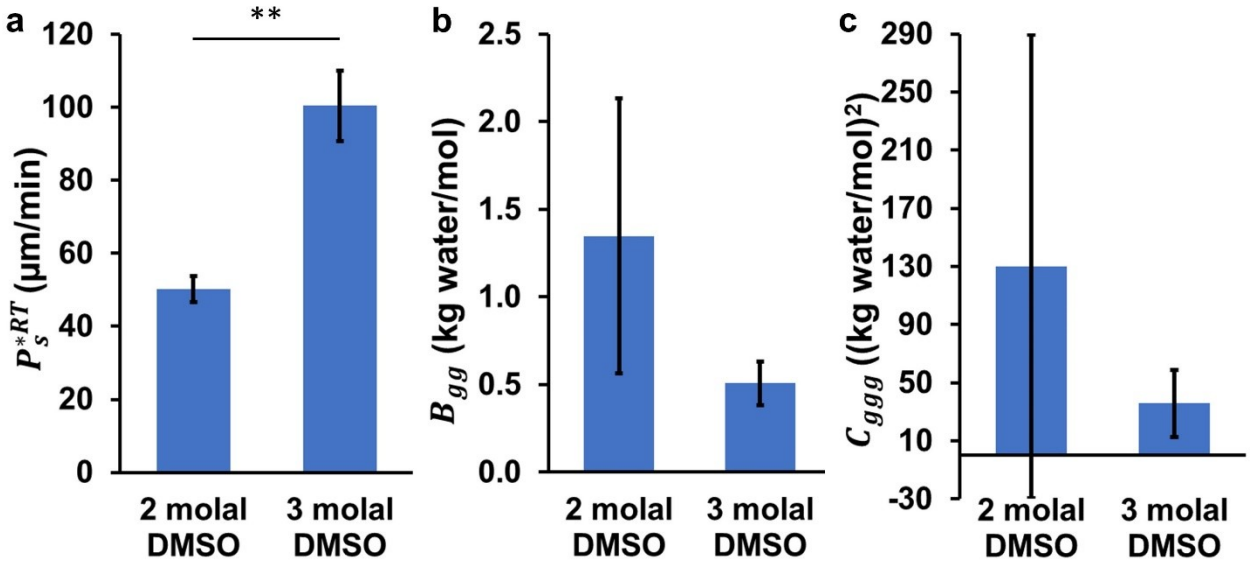

Figure 14. Means and standard deviations of (a) P_s^{*RT}, (b) B_{gg}, and (c) C_{ggg} from separate fittings at 2 and 3 molal DMSO for HUVECs at room temperature. Significance noted as ** for $p < 0.01$.

Table 6. Means ± standard deviations for separate fittings of L_p^{*RT} and b_{RT}^* and P_s^{*RT}, B_{gg}, and C_{ggg} to CPA-free and CPA runs, respectively, at different concentrations of PBS and DMSO for HUVECs at room temperature.

Concentration	L_p^{*RT} $\frac{\mu m}{atm \cdot min}$	b_{RT}^*	P_s^{*RT} $\frac{\mu m}{min}$	B_{gg} $\left(\frac{kg\ water}{mol}\right)$	C_{ggg} $\left(\frac{kg\ water}{mol}\right)^2$
5x PBS (n = 6)	0.347 ± 0.046	0.185 ± 0.017	-	-	-
2x PBS (n = 4)	0.338 ± 0.062	0.160 ± 0.035	-	-	-
6x PBS (n = 3)	0.340 ± 0.000	0.156 ± 0.001	-	-	-
9x PBS (n = 3)	0.313 ± 0.029	0.281 ± 0.012	-	-	-
1 molal DMSO (n = 3)	-	-	65.3 ± 19.2	3.38 ± 5.43	3296 ± 5700
2 molal DMSO (n = 3)	-	-	50.2 ± 3.5	1.35 ± 0.78	130 ± 160
3 molal DMSO (n = 3)	-	-	100 ± 10	0.509 ± 0.124	35.8 ± 23.3

The L_p^{*RT} values for the PBS fittings at different osmolalities are not significantly different. However, the values obtained for b_{RT}^* at varying concentrations of PBS were significantly different, especially when comparing 9x PBS to all other osmolalities of PBS as was expected when analyzing the comparison between the predicted relative cell volume using the parameters from the fitting method and the experimental relative cell volume in Figure 11. When comparing the values for P_s^{*RT} obtained from fitting the 1, 2, and 3 molal DMSO data, the values of 1 versus 3 molal and 2 versus 3 molal were significantly different, while 1 versus 2 molal was not. When B_{gg} and C_{ggg} were included as fitting parameters, only the values for P_s^{*RT} of the 2 and 3 molal DMSO fittings were significantly different, as shown in Figure 14a. This might be due to the larger error range in the values for P_s^{*RT} of the 1 molal DMSO data, as reported in Table 6. The values for P_s^{*RT} at all molalities of DMSO were not significantly different when comparing the fittings that included versus excluded B_{gg} and C_{ggg} as fitting parameters. Lastly, the values obtained for B_{gg} and C_{ggg} at all molalities of DMSO were not significantly different. All statistical significance tests were done using the t-test function in Excel.

Chapter 4. Comparison of Parameters Found to Literature

In the Elliott/McGann research group, over the past two decades there has been a steady transition from modelling the changing cell volume under the ideal and dilute assumption to non-ideal modelling using the Elliott et al. osmotic virial equation. In the early to late 2000s, the osmotic response and solute transport work was done under the ideal and dilute assumption, where the intracellular osmolality is described using the Boyle van 't Hoff equation.[48–50] In the late 2000s to early 2010s, the osmotic response and solute transport work started incorporating the Elliott et al. form of the osmotic virial equation. This form of the osmotic virial equation was used to obtain L_p^* and P_s^* under non-ideal assumptions by expressing the osmolality of solutions in terms of molality by using the second osmotic virial coefficients of DMSO, and the intra- and extracellular impermeant solutes potassium chloride (KCl) and NaCl, respectively. This study does not consider the other impermeant solutes inside cells.[51] Subsequently, the intracellular grouped solute was introduced as a way to combine all impermeant intracellular solutes together and the osmotic virial coefficients for this grouped solute could be obtained with equilibrium cell volume data, which was shown to be mathematically equivalent to including all impermeant intracellular solutes separately in the osmolality calculation.[22,23,26,52] However, the previous work only obtained the second osmotic virial coefficient, B_{gg}, along with the osmotically inactive fraction, b^*, for TF-1 cells and HUVECs[22] and the second and third osmotic virial coefficient, B_{gg} and C_{ggg}, and the osmotically inactive fraction, b^*, for HUVECs[23] because both works only conducted equilibrium cell volume experiments. In this present work, we have shown a new fitting method to find the cell-specific permeability parameters, L_p^* and P_s^*, along with the equilibrium parameters, b^*, B_{gg}, and C_{ggg}, under non-ideal assumptions by conducting kinetic cell volume data and fitting this data to the cell volume models.

We have not found any literature sources that have found the permeability parameters using the grouped solute assumption of the impermeant intracellular solutes. Previous work has found the permeability parameters under non-ideal assumptions, but this work did not include the grouped solute assumption.[51] Zielinksi et al. obtained b^*, B_{gg}, and C_{ggg} for HUVECs, and these values were 0.42, 3.3 $\frac{kg\ water}{mol}$, and 23.9 $\left(\frac{kg\ water}{mol}\right)^2$, respectively, but this was conducted using non-permeating solute data obtained by Lisa Ross-Rodriguez,[23] and upon looking back at Ross-Rodriguez's laboratory notes, it was discovered that this data was done on HUVECs at passages beyond the supplier's recommended doubling time. We conducted some kinetic cell volume runs using HUVECs beyond the recommended doubling time to see if this affects the parameters obtained. Firstly, the cell size distributions were not smooth as is shown in the example in Figure 4, but they were scattered and irregular, which might be an indication that the cells are not healthy anymore. Lastly, when fitting the runs beyond the recommended doubling time to L_p^* and b^* using B_{gg} and C_{ggg} from the new fitting method, the values obtained were about 40% and 70% higher, respectively, than the values obtained for L_p^* and b^* from the new fitting method reported in Table 4. This could mean that the values obtained for B_{gg} and C_{ggg} by Zielinksi et al. are affected by non-permeating solute data that was conducted with cells beyond the recommended doubling time.[23] Ross-Rodriguez et al. also used the same equilibrium cell volume data for HUVECs to fit for b^* and B_{gg}, which were 0.598 and 2.4 $\frac{kg\ water}{mol}$, respectively. However, the same issues with the cells being overgrown arise because the same non-permeating solute equilibrium cell volume data was used.[22] Additionally, as mentioned by Zielinksi et al., Ross-Rodriguez et al. only considered the second osmotic virial coefficient and fit their equations to non-permeating solute equilibrium cell volume data, and the osmotic virial coefficients become much more sensitive

when permeating solutes are involved, leading to imprecise values for b^* and B_{gg}.[23] Thus, neither of the values for b^* and B_{gg} from Ross-Rodriguez et al. and b^*, B_{gg}, and C_{ggg} from Zielinksi et al. can be compared to the values obtained in this work. Because of these reasons, the values obtained in this work are arguably more accurate than the previous values obtained. Additionally, those values where obtained with equilibrium cell volume data, while the values obtained in this work are from kinetic cell volume data.

It is difficult and not very useful to compare the parameters found in this work to parameters that have been previously found using ideal and dilute assumptions, because the equations used for the fittings are different. The ideal and dilute equations consider the difference in the intra- and extracellular concentration of the permeating CPA, while the equation to fit for P_s^* in this work considers the difference in CPA activity as the driving force for diffusion. Parameters from different literature sources that use different equations can only be compared when these parameters and their corresponding equations are used to simulate the changing cell volume to see which parameter and equation set more accurately represent the experimental data. It is important to note that if comparisons between parameters obtained from different literature source are being made when using these parameters to simulate the changing cell volume during cryopreservation that the parameters are used with the corresponding equations. For example, one cannot use a parameter obtained under ideal and dilute assumptions when simulating the changing cell volume with equations in this work, and vice versa. Because this is the first work where permeability parameters are obtained under non-ideal assumptions with the grouped solute assumption for all impermeant intracellular solutes, the parameters found in this work cannot be directly compared to parameters found in other works. The true comparison would be to predict

the changing cell volume during cryopreservation using the parameters and their corresponding equations and see which give the more accurate predictions.

There have been many debates about the effects of permeating solutes on the water permeability of cells. Studies have found contradicting trends, where some show that permeating solutes have been found to increase the cells' water permeability, while other show that it decreases the water permeability.[29] Elmoazzen et al. pointed out that these contradictions might be due to the ideal and dilute assumption made in these studies, as their study used the Elliott et al. form of the osmotic virial equation to express the intra- and extracellular osmolalities in terms of molalities of the permeating CPA, NaCl, and KCl and did not find a significant difference in L_p^* at varying concentrations.[51] As shown in Figure 13a, we have also not found a significant difference in values of L_p^* at varying osmolalities of PBS. Additionally, to see if adding CPA to the solution affects the value of L_p^*, all runs with DMSO were refit separately for L_p^* and P_s^* using b^*, B_{gg}, and C_{ggg} from the new fitting method, and the average L_p^* for all runs was $0.305 \pm 0.037 \frac{\mu m}{atm \cdot min}$. We have found no significant difference when comparing the values of L_p^* in the presence or absence of DMSO. This might further prove that the differences found in previous studies was due to the ideal and dilute assumptions made in those studies.

We have found a significant difference when comparing the values of P_s^* at varying molalities of DMSO. This is also seen in other works where the values of P_s are obtained at different molalities of DMSO using ideal and dilute assumptions, and the results indicate an increase in P_s as molality increases for experiments done at room temperature.[13,33,51] Under non-ideal assumptions, Elmoazzen et al. using the Elliott et al. form of the osmotic virial equation including KCl, NaCl, water and the CPA found that what they called $\tilde{P}$ varied with CPA

concentration.[51] Unfortunately, many studies that find values for P_s using DMSO only evaluate it at one concentration.[14,49,53,54] It also remains difficult to compare trends in other works to trends found in this work, because of the discrepancies in the ideal versus non-ideal assumptions, thus more work is needed to properly assess the effects of CPA concentration on P_s^* using the non-ideal fitting method described in this work.

What might be more comparable are the activation energies obtained for L_p and P_s in this work with previously obtained activation energies for these parameters in other works. Values that have been reported for the activation energies of L_p[18,19,49,55–57] and P_s[18,19,49,57] for different endothelial cells using DMSO as the CPA range from 9.60 to 17.58 $\frac{kcal}{mol}$ and 15.9 to 20.08 $\frac{kcal}{mol}$, respectively, while the values obtained for HUVECs in this work for the activation energies of L_p^* and P_s^* are 11.5 $\frac{kcal}{mol}$ and 23.7 $\frac{kcal}{mol}$, respectively. The value for E_{aL_p} falls within the range, and the value for E_{aP_s} falls just slightly outside of the range seen in previous works. This might be due to the other works using the ideal and dilute assumption or due to the value obtained at a lower DMSO concentration in other works. Lastly, to the author's best knowledge, there are no current publications on permeability or osmotic parameters for H9C2 cells, thus more work is required on this cell type for proper comparison.

Chapter 5. General Discussions and Conclusions

Mathematical modelling is a useful tool to deal with the many variables required to design a successful cryopreservation protocol. Many of these variables depend on how the cell volume changes during cryopreservation and with the addition and removal of CPAs. To understand how the cell volume changes during these processes, the cell-specific permeability parameters of water and the desired CPA, L_p and P_s, respectively, and the osmotically inactive fraction, b, of the cells must be known. Previous studies found these parameters for different cell types, but these were done under ideal and dilute assumptions. The Elliott et al. form of the osmotic virial equation allows us to model the changing cell volume under non-ideal thermodynamic assumptions, which adds two additional cell-specific parameters to the model, the second and third osmotic virial coefficients of the intracellular grouped solute, B_{gg} and C_{ggg}, respectively. This grouped solute is based on the assumption that all intracellular non-permeating solutes can be grouped together. Thus, the total number of cell-specific parameters required to model the changing cell volume during cryopreservation are L_p^*, P_s^*, b^*, B_{gg}, and C_{ggg} (with the asterisks differentiating these parameters from those found by others using ideal assumptions). These can be obtained by fitting thermodynamic equations to kinetic cell volume data using a non-permeating and a permeating CPA. Additionally, the parameters L_p^* and P_s^* are temperature dependent, and therefore, these kinetic cell volume data are required at different temperatures.

In this work, we have presented a novel fitting method to find the five cell-specific parameters at room temperature using two different cell types, HUVECs and H9C2 cells. First, the experiments were conducted with 5x PBS as the non-permeating solute and 3 molal DMSO as the permeating CPA using a Coulter® particle size counter. The experimental runs were converted to relative volume versus time and separately fit for the time gaps, or the time between t_0 and t_1, of

each run, and the runs of each type of solute were combined. Next, the novel fitting method was used by iteratively fitting for L_p^* and b^* using the combined 5x PBS runs and B_{gg}, C_{ggg}, and P_s^* using the combined 3 molal DMSO runs at room temperature starting with $B_{gg} = C_{ggg} = 0$. For both HUVECs and H9C2 cells, this iterative fitting method converged to the final five cell-specific parameters at room temperature. Then, the experimental runs at 4 °C were also fitted for the time gaps separately, and the values for L_p^* and P_s^* were represented using the Arrhenius equations with temperature as a function of time. The experimental runs of 5x PBS at 4 °C were fit to the activation energy of L_p^*, E_{aL_p}, and b^*, because the values obtained for b^* for H9C2 cells at 4 °C were significantly different than those at room temperature. The experimental runs of 3 molal DMSO were fit to the activation energy of P_s^*, E_{aP_s}. The fittings at 4 °C used L_p^{*RT} and P_s^{*RT} from the new fitting method at room temperature as reference values for the Arrhenius equation, and B_{gg} and C_{ggg} from the new fitting method as well. The details of this novel fitting method were figured out using HUVECs and the same method was repeated for H9C2 cells in a fraction of the time, thus allowing for a fast and efficient way to determine the desired cell-specific parameters to model the changing cell volume during cryopreservation.

Additionally, the values obtained during the fitting method were used to predict the changing volume of experimental runs conducted at additional concentrations of PBS and DMSO for HUVECs at room temperature. The predictions using L_p^{*RT} for 2x PBS, 6x PBS, and 9x PBS were accurate, but b_{RT}^* was slightly overestimating the shrinking that occurred, especially for the 9x PBS runs. The predictions using P_s^{*RT} were not very accurate, and when fitting the 1 and 2 molal DMSO runs to P_s^{*RT}, both when including and excluding B_{gg} and C_{ggg} as fitting parameters, the values were lower than the value obtained from the fitting method using 3 molal DMSO. This

might be an indication that P_S^* is concentration dependent, but more work is needed to investigate the dependence.

A minor limitation of this work is the duration of experimental run available using the Coulter counter. Because the level of the solution in the vials lowers during the experimental run, the total duration can only be about 4 minutes. The runs at 4 °C, particularly the CPA experiments, do not reach equilibrium in this time and would require about 16 minutes to capture a more detailed depiction of the equilibrium.

The focus of this work is not the cell types chosen, and not necessarily the final numbers obtained for these cell types either, but the novel fitting method used. This method can now be implemented for different cell types, and future work would benefit from the final true comparison, which would be using the numbers found with this method along with the non-ideal equations to simulate the cell volume during cryopreservation versus simulating the changing cell volume with parameters found under the ideal and dilute assumption and the different equations used with this assumption and compare these predictions to experimental data.

References

1. Jiang, Z., Hu, X., Kretlow, J. D. & Liu, N. Harvesting and cryopreservation of lymphatic endothelial cells for lymphatic tissue engineering. *Cryobiology* **60**, 177–183 (2010).

2. Šćekić, I. *et al.* A novel strategy for conservation of European eel (Anguilla anguilla) genetic resources: Cryopreservation of ovarian stem cells. *Cryobiology* **95**, 151–156 (2020).

3. Fuller, B. & Paynter, S. Fundamentals of cryobiology in reproductive medicine. *Reprod. Biomed. Online* **9**, 680–691 (2004).

4. Muldrew, K., Acker, J. P., Elliott, J. A. W. & McGann, L. E. *The Water to Ice Transition: Implications for Living Cells*. *Life in the Frozen State* (CRC Press LLC, 2004).

5. Mazur, P., Leibo, S. P. & Chu, E. H. Y. A two-factor hypothesis of freezing injury. *Exp. Cell Res.* **71**, 345–355 (1972).

6. Mazur, P. Kinetics of water loss from cells at subzero temperatures and the likelihood of intracellular freezing. *J. Gen. Physiol.* **47**, 347–369 (1963).

7. Elliott, G. D., Wang, S. & Fuller, B. J. Cryoprotectants: A review of the actions and applications of cryoprotective solutes that modulate cell recovery from ultra-low temperatures. *Cryobiology* **76**, 74–91 (2017).

8. Ali, J. & Shelton, J. N. Design of vitrification solutions for the cryopreservation of embryos. *J. Reprod. Fertil.* **99**, 471–477 (1993).

9. Elmoazzen, H. Y. *et al.* Dimethyl sulfoxide toxicity kinetics in intact articular cartilage. *Cell Tissue Bank.* **8**, 125–133 (2007).

10. Almansoori, K. A. *et al.* Cryoprotective agent toxicity interactions in human articular chondrocytes. *Cryobiology* **64**, 185–191 (2012).

11. Fahy, G. M. Cryoprotectant toxicity neutralization. *Cryobiology* **60**, S45–S53 (2010).

12. McGann, L. E. Differing actions of penetrating and nonpenetrating cryoprotective agents. *Cryobiology* **15**, 382–390 (1978).

13. Xu, Y., Zhang, L., Xu, J., Wei, Y. & Xu, X. Membrane permeability of the human pluripotent stem cells to Me 2SO, glycerol and 1,2-propanediol. *Arch. Biochem. Biophys.* **550**–**551**, 67–76 (2014).

14. Vian, A. M. & Higgins, A. Z. Membrane permeability of the human granulocyte to water, dimethyl sulfoxide, glycerol, propylene glycol and ethylene glycol. *Cryobiology* **68**, 35–42 (2014).

15. Marquez-Curtis, L. A., Dorobantu, L. S., Sauvageau, D. & Elliott, J. A. W. Cryopreservation of swine colostrum-derived cells. *Cryobiology* **97**, 168–178 (2020).

16. Jacobs, M. H. & Stewart, D. R. A simple method for the quantitative measurement of cell permeability. *J. Cell. Comp. Physiol.* **1**, 71–82 (1932).

17. Shu, Z. *et al.* A study of the osmotic characteristics, water permeability, and cryoprotectant permeability of human vaginal immune cells. *Cryobiology* **72**, 93–99 (2016).

18. Niu, D., Zhao, G., Liu, X., Zhou, P. & Cao, Y. Prevention of osmotic injury to human umbilical vein endothelial cells for biopreservation: A first step toward biobanking of endothelial cells for vascular tissue engineering. *Tissue Eng. - Part C Methods* **22**, 270–

279 (2016).

19. Fry, A. K. & Higgins, A. Z. Measurement of cryoprotectant permeability in adherent endothelial cells and applications to cryopreservation. *Cell. Mol. Bioeng.* **5**, 287–298 (2012).

20. Gilmore, J. A. *et al.* Effect of cryoprotectant solutes on water permeability of human spermatozoa. *Biol. Reprod.* **53**, 985–995 (1995).

21. Gilmore, J. A. *et al.* Fundamental cryobiology of selected African mammalian spermatozoa and its role in biodiversity preservation through the development of genome resource banking. *Anim. Reprod. Sci.* **53**, 277–297 (1998).

22. Ross-Rodriguez, L. U., Elliott, J. A. W. & McGann, L. E. Non-ideal solution thermodynamics of cytoplasm. *Biopreserv. Biobank.* **10**, 462–471 (2012).

23. Zielinski, M. W., McGann, L. E., Nychka, J. A. & Elliott, J. A. W. Measurement of grouped intracellular solute osmotic virial coefficients. *Cryobiology* **97**, 198–216 (2020).

24. McMillan, W. G. & Mayer, J. E. The statistical thermodynamics of multicomponent systems. *J. Chem. Phys.* **13**, 276–305 (1945).

25. Elliott, J. A. W., Prickett, R. C., Elmoazzen, H. Y., Porter, K. R. & McGann, L. E. A multisolute osmotic virial equation for solutions of interest in biology. *J. Phys. Chem. B* **111**, 1775–1785 (2007).

26. Zielinski, M. W., McGann, L. E., Nychka, J. A. & Elliott, J. A. W. Nonideal solute chemical potential equation and the validity of the grouped solute approach for intracellular solution thermodynamics. *J. Phys. Chem. B* **121**, 10443–10456 (2017).

27. Prickett, R. C., Elliott, J. A. W. & McGann, L. E. Application of the osmotic virial equation in cryobiology. *Cryobiology* **60**, 30–42 (2010).

28. Zielinski, M. W., McGann, L. E., Nychka, J. A. & Elliott, J. A. W. Comparison of non-ideal solution theories for multi-solute solutions in cryobiology and tabulation of required coefficients. *Cryobiology* **69**, 305–317 (2014).

29. McGrath, J. J. Quantitative measurement of cell membrane transport: Technology and applications. *Cryobiology* **34**, 315–334 (1997).

30. Levin, S. W., Levin, R. L. & Solomon, A. K. Improved stop-flow apparatus to measure permeability of human red cells and ghosts. *J. Biochem. Biophys. Methods* **3**, 255–272 (1980).

31. Terwilliger, T. C. & Solomon, A. K. Osmotic water permeability of human red cells. *J. Gen. Physiol.* **77**, 549–570 (1981).

32. Elmoazzen, H. Y., Elliott, J. A. W. & McGann, L. E. The effect of temperature on membrane hydraulic conductivity. *Cryobiology* **45**, 68–79 (2002).

33. Fedorow, C. *et al.* Osmotic and cryoprotectant permeation characteristics of islet cells isolated from the newborn pig pancreas. *Cell Transplant.* **10**, 651–659 (2001).

34. Diller, K. R. & Bradley, D. A. Measurement of the water permeability of single human granulocytes on a microscopic stopped-flow mixing system. *J. Biomech. Eng.* **106**, 384–393 (1984).

35. Gao, D. Y. *et al.* Membrane transport properties of mammalian oocytes: A micropipette perfusion technique. *J. Reprod. Fertil.* **102**, 385–392 (1994).

36. Gao, D. Y. *et al.* Development of a novel microperfusion chamber for determination of cell membrane transport properties. *Biophys. J.* **71**, 443–450 (1996).

37. Eskandari, N., Marquez-Curtis, L. A., McGann, L. E. & Elliott, J. A. W. Cryopreservation of human umbilical vein and porcine corneal endothelial cell monolayers. *Cryobiology* **85**, 63–72 (2018).

38. Kimes, B. W. & Brandt, B. L. Properties of a clonal muscle cell line from rat heart. *Exp. Cell Res.* **98**, 367–381 (1976).

39. Tanaka, M., Girard, G., Davis, R., Peuto, A. & Bignell, N. Recommended table for the density of water between 0 °C and 40 °C based on recent experimental reports. *Metrologia* **38**, 301–309 (2001).

40. Dimethyl Sulfoxide Physical Properties. *Gaylord Chemical Company, L.L.C.* 1–14 https://www.gaylordchemical.com/wp-content/uploads/2015/09/GC-Literature-101B-REV.pdf?x19929 (2014).

41. Values of the Gas Constant in Different Unit Systems. in *CRC Handb. Chem. Phys. (Internet Version)* (ed. Rumble, J.) (CRC Press/Taylor & Francis, 2019).

42. Physical Constants of Inorganic Compounds. in *CRC Handb. Chem. Phys. (Internet Version)* (ed. Rumble, J.) (CRC Press/Taylor & Francis, 2019).

43. Physical Constants of Organic Compounds. in *CRC Handb. Chem. Phys. (Internet Version)* (ed. Rumble, J.) (CRC Press/Taylor & Francis, 2019).

44. McGann, L. E., Turner, A. R. & Turc, J. M. Microcomputer interface for rapid measurements of average volume using an electronic particle counter. *Med. Biol. Eng.*

Comput. **20**, 117–120 (1982).

45. Elmoazzen, H. Y., Chan, C. C. V., Acker, J. P., Elliott, J. A. W. & McGann, L. E. The effect of cell size distribution on predicted osmotic responses of cells. *Cryo-Letters* **26**, 147–158 (2005).

46. MathWorks. Choose an ODE solver. *MathWorks* https://www.mathworks.com/help/matlab/math/choose-an-ode-solver.html.

47. Moler, C. Stiff Differential Equations. *MathWorks* https://www.mathworks.com/company/newsletters/articles/stiff-differential-equations.html doi:10.1007/3-540-26820-0_4.

48. Ebertz, S. L. & McGann, L. E. Osmotic parameters of cells from a bioengineered human corneal equivalent and consequences for cryopreservation. *Cryobiology* **45**, 109–117 (2002).

49. Ebertz, S. L. & McGann, L. E. Cryoprotectant permeability parameters for cells used in a bioengineered human corneal equivalent and applications for cryopreservation. *Cryobiology* **49**, 169–180 (2004).

50. Ross-Rodriguez, L. U., Elliott, J. A. W. & McGann, L. E. Characterization of cryobiological responses in TF-1 cells using interrupted freezing procedures. *Cryobiology* **60**, 106–116 (2010).

51. Elmoazzen, H. Y., Elliott, J. A. W. & McGann, L. E. Osmotic transport across cell membranes in nondilute solutions: A new nondilute solute transport equation. *Biophys. J.* **96**, 2559–2571 (2009).

52. Prickett, R. C., Elliott, J. A. W., Hakda, S. & McGann, L. E. A non-ideal replacement for the Boyle van't Hoff equation. *Cryobiology* **57**, 130–136 (2008).

53. Karlsson, J. O. M., Younis, A. I., Chan, A. W. S., Gould, K. G. & Eroglu, A. Permeability of the rhesus monkey oocyte membrane to water and common cryoprotectants. *Mol. Reprod. Dev.* **76**, 321–333 (2009).

54. Agca, Y. *et al.* Chimpanzee (Pan troglodytes) spermatozoa osmotic tolerance and cryoprotectant permeability characteristics. *J. Androl.* **26**, 470–477 (2005).

55. Zhang, A., Xu, L. X., Sandison, G. A. & Cheng, S. Morphological study of endothelial cells during freezing. *Phys. Med. Biol.* **51**, 6047–6060 (2006).

56. Zhao, G., Kurata, K. & Takamatsu, H. Measurement of membrane hydraulic conductivity of bovine carotid artery endothelial cells using a perfusion microscope. *Cryo-Letters* **33**, 231–239 (2012).

57. Wusteman, M. C. & Pegg, D. E. Differences in the requirements for cryopreservation of porcine aortic smooth muscle and endothelial cells. *Tissue Eng.* **7**, 507–518 (2001).

Appendix

Table A1. Iterative results of the new fitting method for HUVECs. L_p' and P_s' are the nondimensional parameters obtained by fitting to relative volume data prior to being made dimensional with Equations 31 and 32. Initial guess of iteration step 2 is different from the other fittings to accommodate the starting point of B_{gg} and C_{ggg} set to zero. Final converged parameters are bolded.

Iteration Step	Input/ output	L_p' $(atm \cdot min)^{-1}$	b_{RT}^*	P_s' $(min)^{-1}$	B_{gg} $\frac{kg\ water}{mol}$	C_{ggg} $\left(\frac{kg\ water}{mol}\right)^2$
1	input	ig: 0.03	ig: 0.3	-	0	0
	output	0.02608	0.4675	-	-	-
2	input	0.02608	0.4675	ig: 5	ig: 0.1	ig: 2
	output	-	-	2.816	0.1331	5.483
3	input	ig: 0.03	ig: 0.3	-	0.1331	5.483
	output	0.02652	0.2809	-	-	-
4	input	0.02652	0.2809	ig: 5	ig: 0.2	ig: 5
	output	-	-	6.029	0.3952	18.86
5	input	ig: 0.03	ig: 0.3	-	0.3952	18.86
	output	0.02703	0.2068	-	-	-
6	input	0.02703	0.2068	ig: 5	ig: 0.2	ig: 5
	output	-	-	7.448	0.4714	27.04
7	input	ig: 0.03	ig: 0.3	-	0.4714	27.04
	output	0.02717	0.1863	-	-	-
8	input	0.02717	0.1863	ig: 5	ig: 0.2	ig: 5
	output	-	-	7.861	0.4887	29.30
9	input	ig: 0.03	ig: 0.3	-	0.4887	29.30
	output	0.02720	0.1819	-	-	-
10	input	0.02720	0.1819	ig: 5	ig: 0.2	ig: 5
	output	-	-	7.944	0.4935	29.96
11	input	ig: 0.03	ig: 0.3	-	0.4935	29.96
	output	0.02721	0.1807	-	-	-
12	input	0.02721	0.1807	ig: 5	ig: 0.2	ig: 5
	output	-	-	7.967	0.4950	30.16
13	input	ig: 0.03	ig: 0.3	-	0.4950	30.16
	output	0.02721	0.1803	-	-	-
14	input	0.02721	0.1803	ig: 5	ig: 0.2	ig: 5
	output	-	-	7.973	0.4955	30.23
15	input	ig: 0.03	ig: 0.3	-	0.2165	16.7628
	output	0.02721	0.1802	-	-	-

Table A1 continued.

Iteration Step	Input/ output	L_p' $(atm \cdot min)^{-1}$	b_{RT}^*	P_s' $(min)^{-1}$	B_{gg} $\frac{kg\ water}{mol}$	C_{ggg} $\left(\frac{kg\ water}{mol}\right)^2$
16	input	0.02721	0.1802	ig: 5	ig: 0.2	ig: 5
	output	-	-	7.975	0.4956	30.24
17	input	ig: 0.03	ig: 0.3	-	0.4956	30.24
	output	0.02721	0.1802	-	-	-
18	input	0.02721	0.1802	ig: 5	ig: 0.2	ig: 5
	output	-	-	7.976	0.4956	30.25
19	input	ig: 0.03	ig: 0.3	-	0.4956	30.25
	output	0.02721	0.1801	-	-	-
20	input	0.02721	0.1801	ig: 5	ig: 0.2	ig: 5
	output	-	-	**7.976**	**0.4956**	**30.25**
21	input	ig: 0.03	ig: 0.3	-	0.4956	30.25
	output	**0.02721**	**0.1801**	-	-	-

Table A2. Iterative results of the new fitting method for H9C2 cells. L_p' and P_s' are the nondimensional parameters obtained by fitting to relative volume data prior to being made dimensional with Equations 31 and 32. Initial guess of iteration step 2 is different from the other fittings to accommodate the starting point of B_{gg} and C_{ggg} set to zero. Final converged parameters are bolded.

Iteration Step	Input/ output	L_p' $(atm \cdot min)^{-1}$	b_{RT}^*	P_s' $(min)^{-1}$	B_{gg} $\frac{kg\ water}{mol}$	C_{ggg} $\left(\frac{kg\ water}{mol}\right)^2$
1	input	ig: 0.03	ig: 0.3	-	0	0
	output	0.03656	0.3336	-	-	-
2	input	0.03656	0.3336	ig: 5	ig: 0.1	ig: 2
	output	-	-	3.035	0.1958	3.227
3	input	ig: 0.03	ig: 0.3	-	0.1958	3.227
	output	0.03694	0.1391	-	-	-
4	input	0.03694	0.1391	ig: 5	ig: 0.2	ig: 5
	output	-	-	6.870	0.3401	6.825
5	input	ig: 0.03	ig: 0.3	-	0.3401	6.825
	output	0.03739	0.08264	-	-	-

Table A2 continued.

Iteration Step	Input/ output	L'_p $(atm \cdot min)^{-1}$	b^*_{RT}	P'_s $(min)^{-1}$	B_{gg} $\frac{kg\ water}{mol}$	C_{ggg} $\left(\frac{kg\ water}{mol}\right)^2$
6	input	0.03739	0.08264	ig: 5	ig: 0.2	ig: 5
	output	-	-	8.081	0.3655	8.134
7	input	ig: 0.03	ig: 0.3	-	0.3655	8.134
	output	0.03750	0.06907	-	-	-
8	input	0.03750	0.06907	ig: 5	ig: 0.2	ig: 5
	output	-	-	8.348	0.3736	8.594
9	input	ig: 0.03	ig: 0.3	-	0.3736	0.3736
	output	0.03753	0.06482	-	-	-
10	input	0.03753	0.06482	ig: 5	ig: 0.2	ig: 5
	output	-	-	8.432	0.3762	8.742
11	input	ig: 0.03	ig: 0.3	-	0.3762	8.742
	output	0.03754	0.06350	-	-	-
12	input	0.03754	0.06350	ig: 5	ig: 0.2	ig: 5
	output	-	-	8.459	0.3769	8.784
13	input	ig: 0.03	ig: 0.3	-	0.3769	8.784
	output	0.03754	0.06313	-	-	-
14	input	0.03754	0.06313	ig: 5	ig: 0.2	ig: 5
	output	-	-	8.466	0.3771	8.797
15	input	ig: 0.03	ig: 0.3	-	0.3771	8.797
	output	0.03754	0.06302	-	-	-
16	input	0.03754	0.06302	ig: 5	ig: 0.2	ig: 5
	output	-	-	8.468	0.3772	8.800
17	input	ig: 0.03	ig: 0.3	-	0.3772	8.800
	output	0.03755	0.06299	-	-	-
18	input	0.03755	0.06299	ig: 5	ig: 0.2	ig: 5
	output	-	-	8.469	0.3772	8.801
19	input	ig: 0.03	ig: 0.3	-	0.3772	8.801
	output	0.03755	0.06298	-	-	-
20	input	0.03755	0.06298	ig: 5	ig: 0.2	ig: 5
	output	-	-	8.469	0.3772	8.802
21	input	ig: 0.03	ig: 0.3	-	0.3772	8.802
	output	0.03755	0.06298	-	-	-
22	input	0.03755	0.06298	ig: 5	ig: 0.2	ig: 5
	output	-	-	8.469	0.3772	8.802
23	input	ig: 0.03	ig: 0.3	-	0.3772	8.802
	output	0.03755	0.06297	-	-	-

Table A2 continued.

Iteration Step	Input/ output	L'_p $(atm \cdot min)^{-1}$	b^*_{RT}	P'_s $(min)^{-1}$	B_{gg} $\frac{kg\ water}{mol}$	C_{ggg} $\left(\frac{kg\ water}{mol}\right)^2$
24	input	0.03755	0.06297	ig: 5	ig: 0.1	ig: 2
	output	-	-	**8.469**	**0.3772**	**8.802**
25	input	ig: 0.03	ig: 0.3	-	0.3772	8.802
	output	**0.03755**	**0.06297**	-	-	-

Table A3. Measured temperatures before (T_i) and after (T_f) each experimental run at 4 °C.

Run ID	T_i ℃	T_f ℃
H0625P51	2.1	7.7
H0702P51	0.8	5.6
H0702P52	0.8	5.4
H0716C33	2	9
H0716C34	1.4	6.6
H0716C35	0.8	8.2
H0716C36	1.6	8.4
C0811P51	0.7	7.4
C0811P52	1.1	6.3
C0811P53	0.8	7.0
C0811P54	1.5	6.3
C0917C31	2.2	9.1
C0917C32	1.4	11
C0917C33	1.1	8.4
C0917C34	1.1	9.1

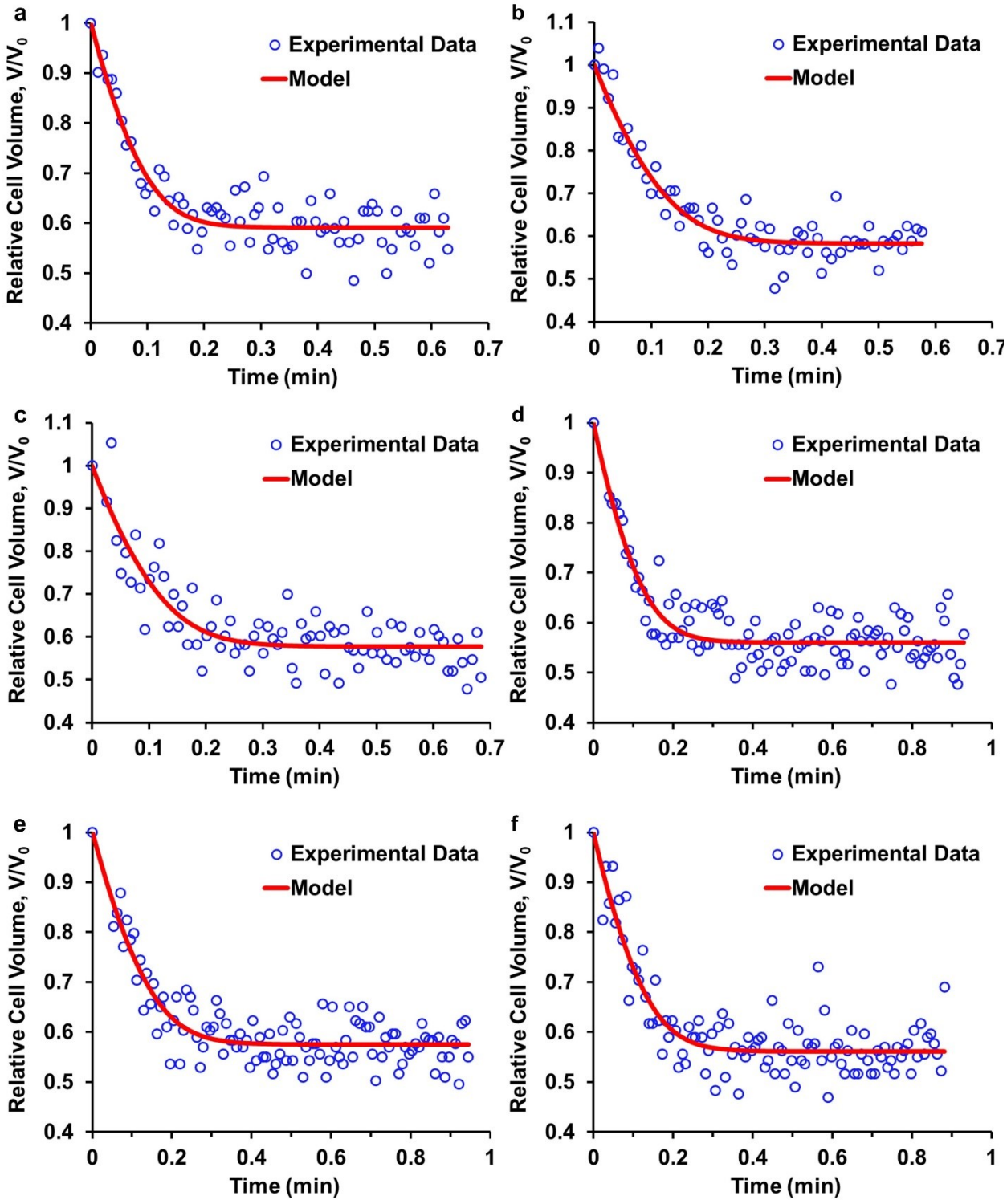

Figure A1. Separate fittings for experimental runs of HUVECs in 5x PBS at room temperature. Fitting parameters were L_p^{*RT} and b_{RT}^*. Run IDs: (a) H1024P51, (b) H1024P53, (c) H1024P54, (d) H1105P51, (e) H1105P52, (f) H1105P53.

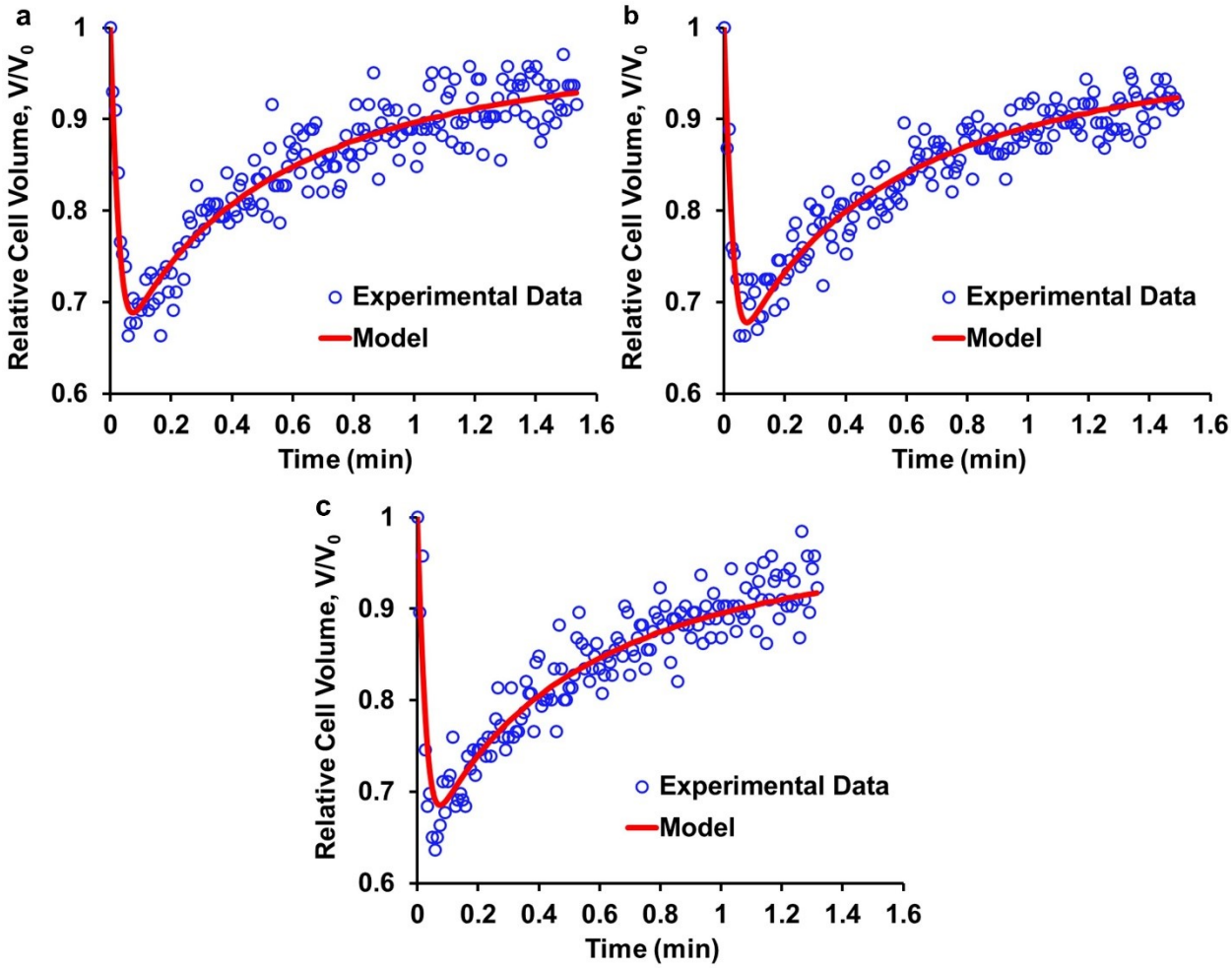

Figure A2. Separate fittings for experimental runs of HUVECs in 3 molal DMSO. Fitting parameter was P_s^{*RT} using B_{gg} and C_{ggg} from the fitting method at room temperature. Run IDs: (a) H0228C31, (b) H0228C32, (c) H0228C33.

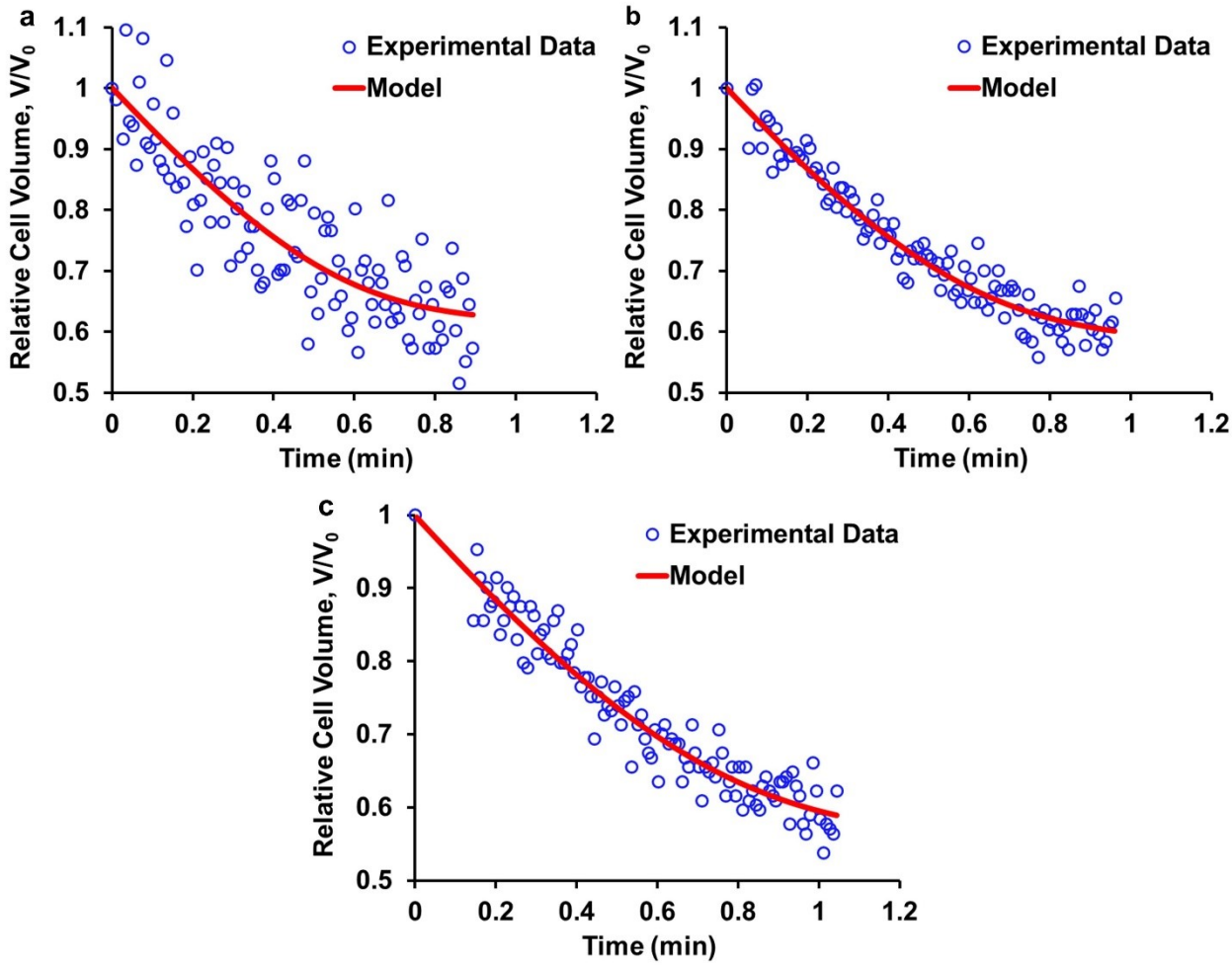

Figure A3. Separate fittings for experimental runs of HUVECs in 5x PBS at 4 °C. Fitting parameters were E_{aL_p} and b_{4C}^{*}. Run IDs: (a) H0625P51, (b) H0702P51, (c) H0702P52.

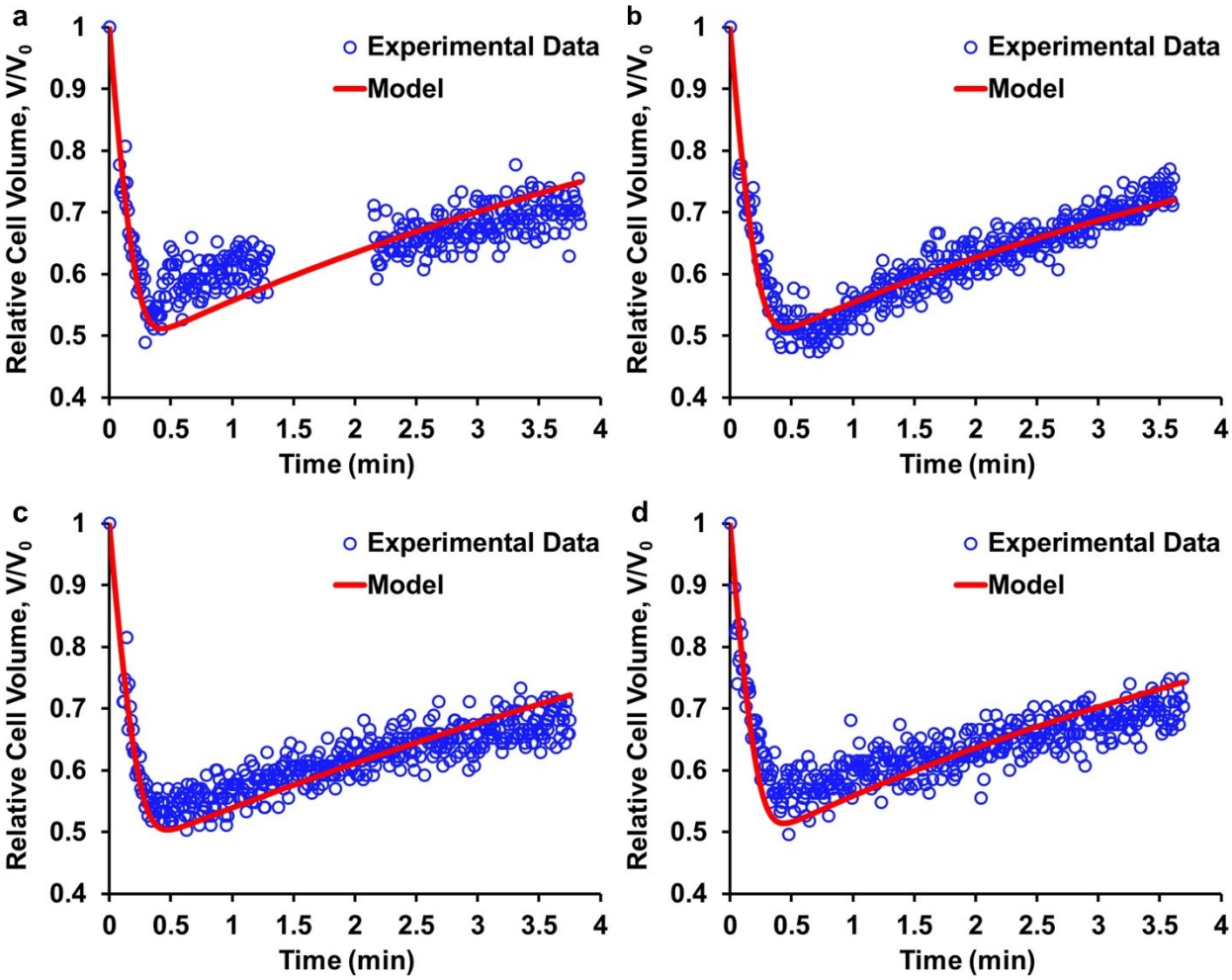

Figure A4. Separate fittings for experimental runs of HUVECs in 3 molal DMSO at 4 °C. Fitting parameter was E_{aP_s}. Run IDs: (a) H0716C33, (b) H0716C34†, (c) H0716C35†, (d) H0716C36†. Notation of † to report the DMSO runs using the second bottle that require no filtering as explained in Section 2.1.2.

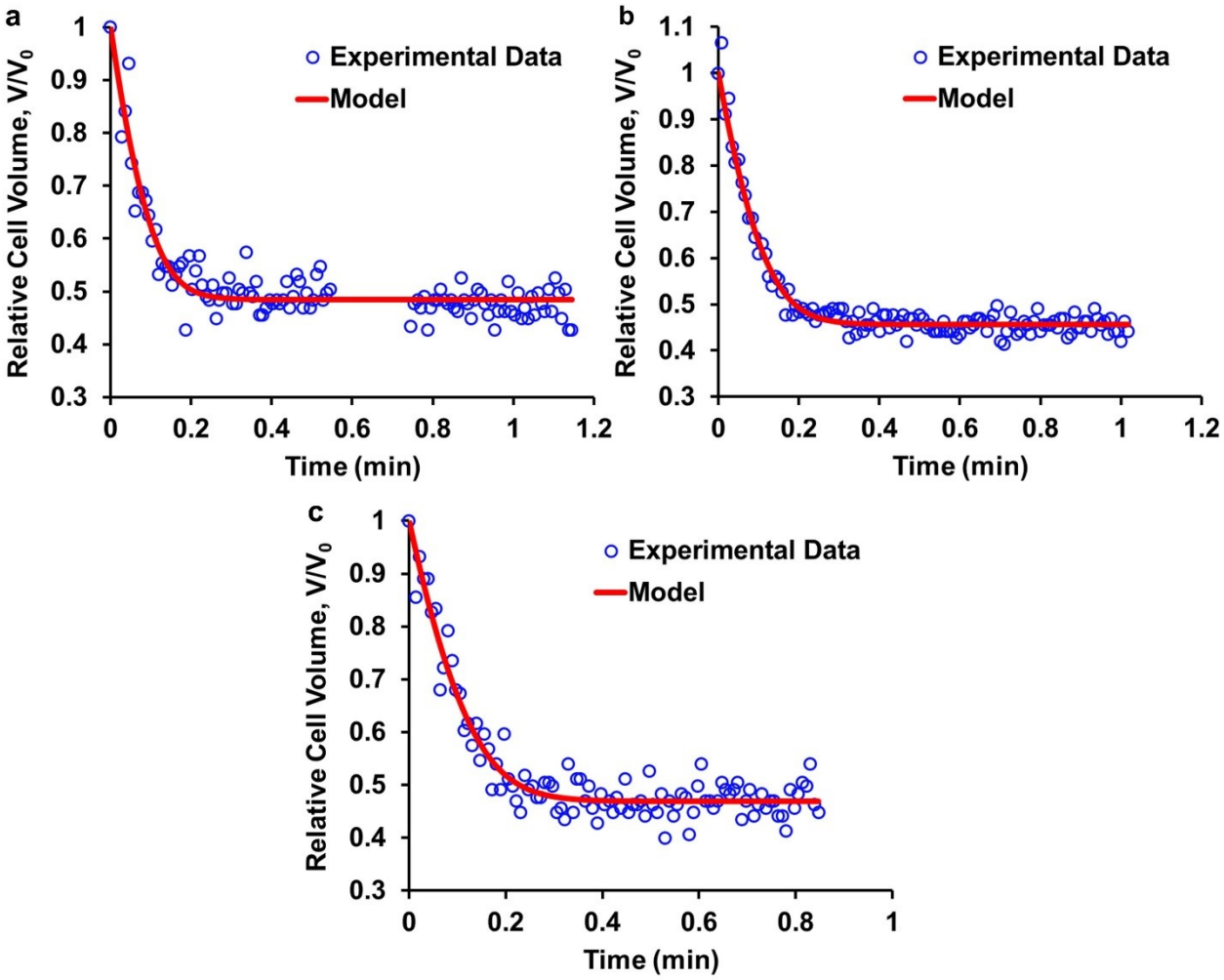

Figure A5. Separate fittings for experimental runs of H9C2 cells in 5x PBS at room temperature. Fitting parameters were L_p^{*RT} and b_{RT}^*. Run IDs: (a) C0807P51, (b) C0807P52, (c) C0807P53.

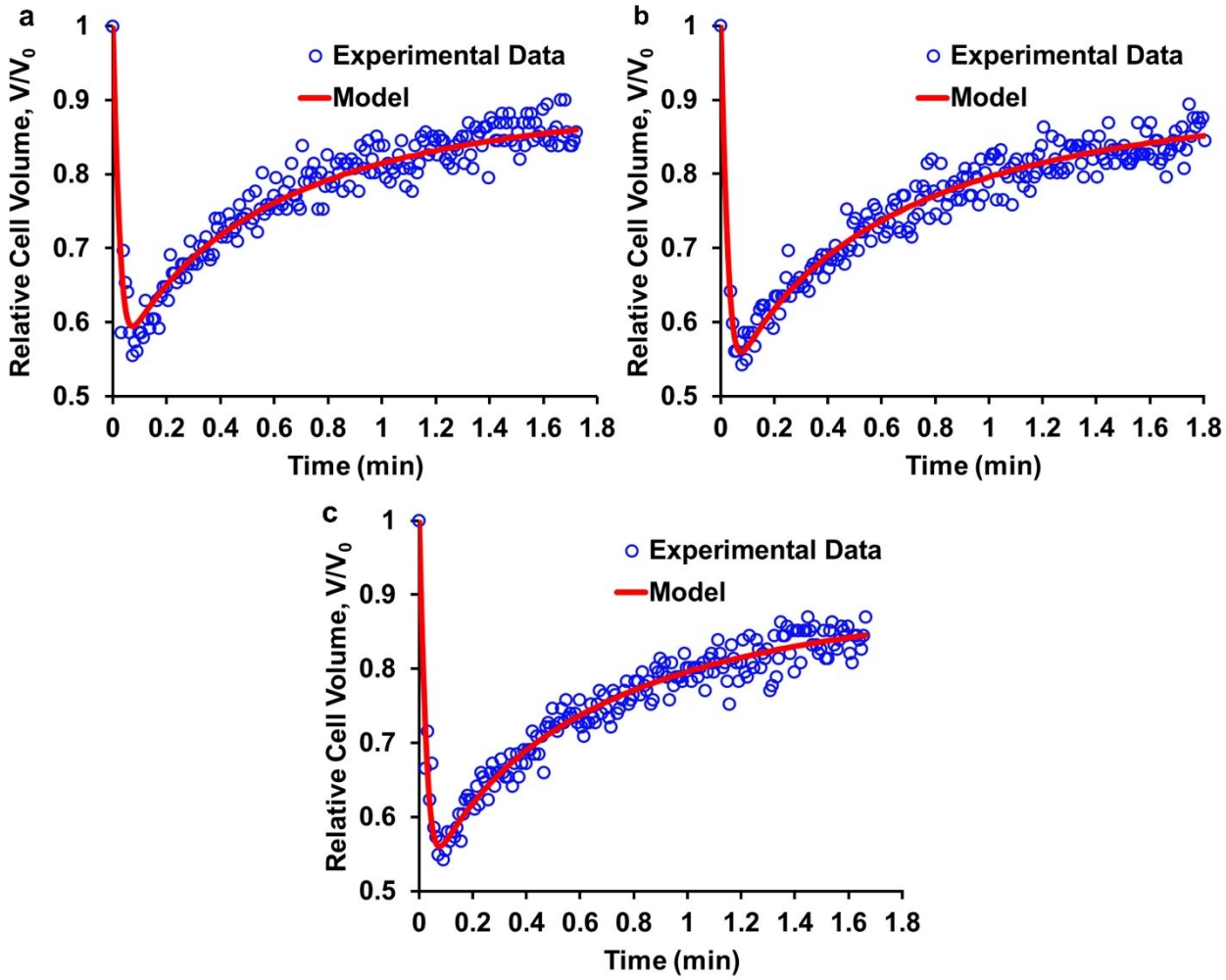

Figure A6. Separate fittings for experimental runs of H9C2 cells in 3 molal DMSO at room temperature. Fitting parameter was P_s^{*RT}. Run IDs: (a) C0814C31†, (b) C0814C32†, (c) C0814C33†. Notation of † to report the DMSO runs using the second bottle that require no filtering as explained in Section 2.1.2.

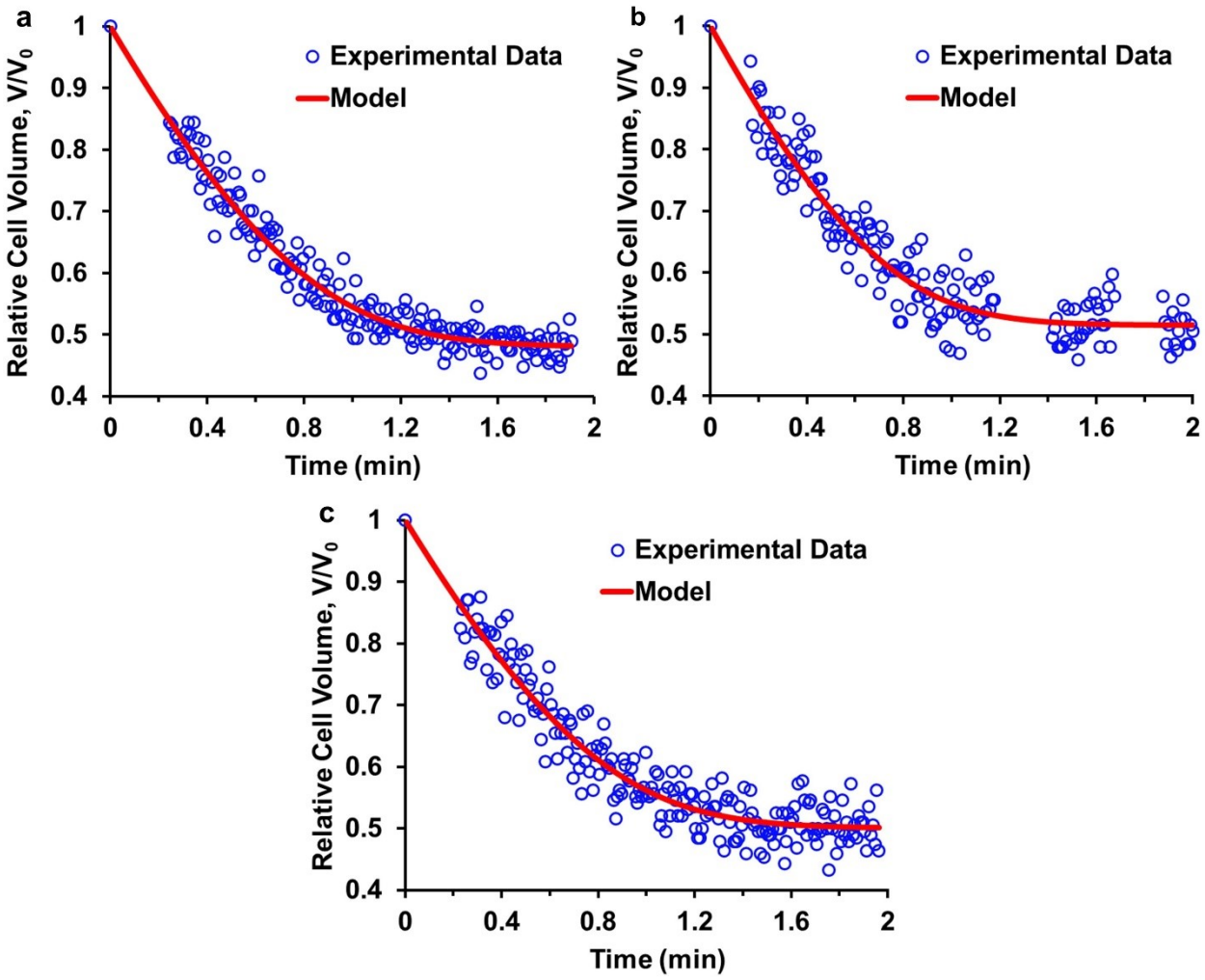

Figure A7. Separate fittings for experimental runs of H9C2 cells in 5x PBS at 4 °C. Fitting parameters were E_{aL_p} and b^*_{4C}. Run IDs: (a) C0811P52, (b) C0811P53, (c) C0811P54.

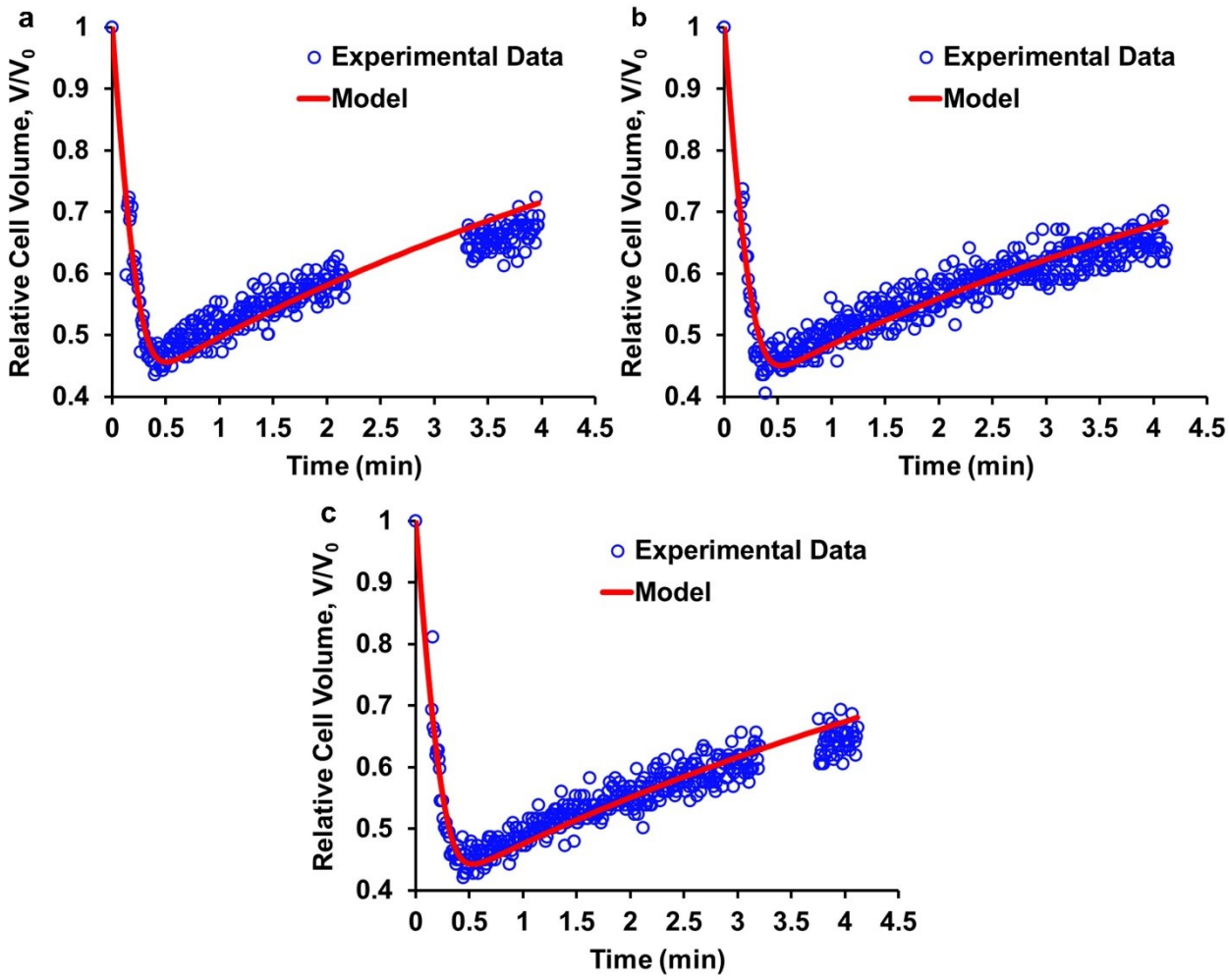

Figure A8. Separate fittings for experimental runs of H9C2 cells in 3 molal DMSO at 4 °C. Fitting parameter was E_{aP_s}. Run IDs: (a) C0917C32†, (b) C0917C33†, (c) C0917C34†. Notation of † to report the DMSO runs using the second bottle that require no filtering as explained in Section 2.1.2.

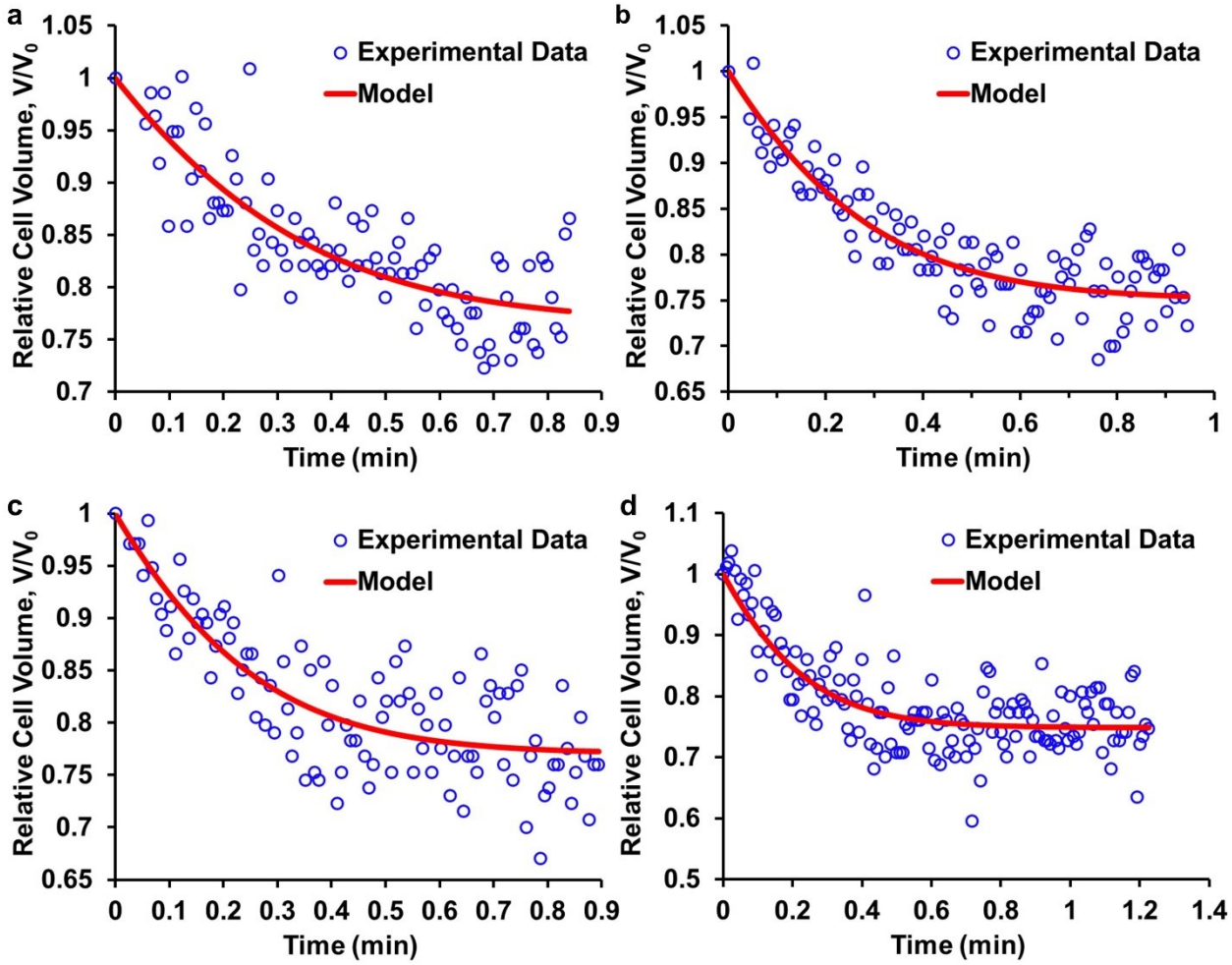

Figure A9. Separate fittings of 2x PBS runs using HUVECs at room temperature. Fitting parameters were L_p^{*RT} and b_{RT}^{*} using B_{gg} and C_{ggg} from the new fitting method. Run IDs: (a) H1025P21, (b) H1025P22, (c) H1025P23, (d) H1105P21.

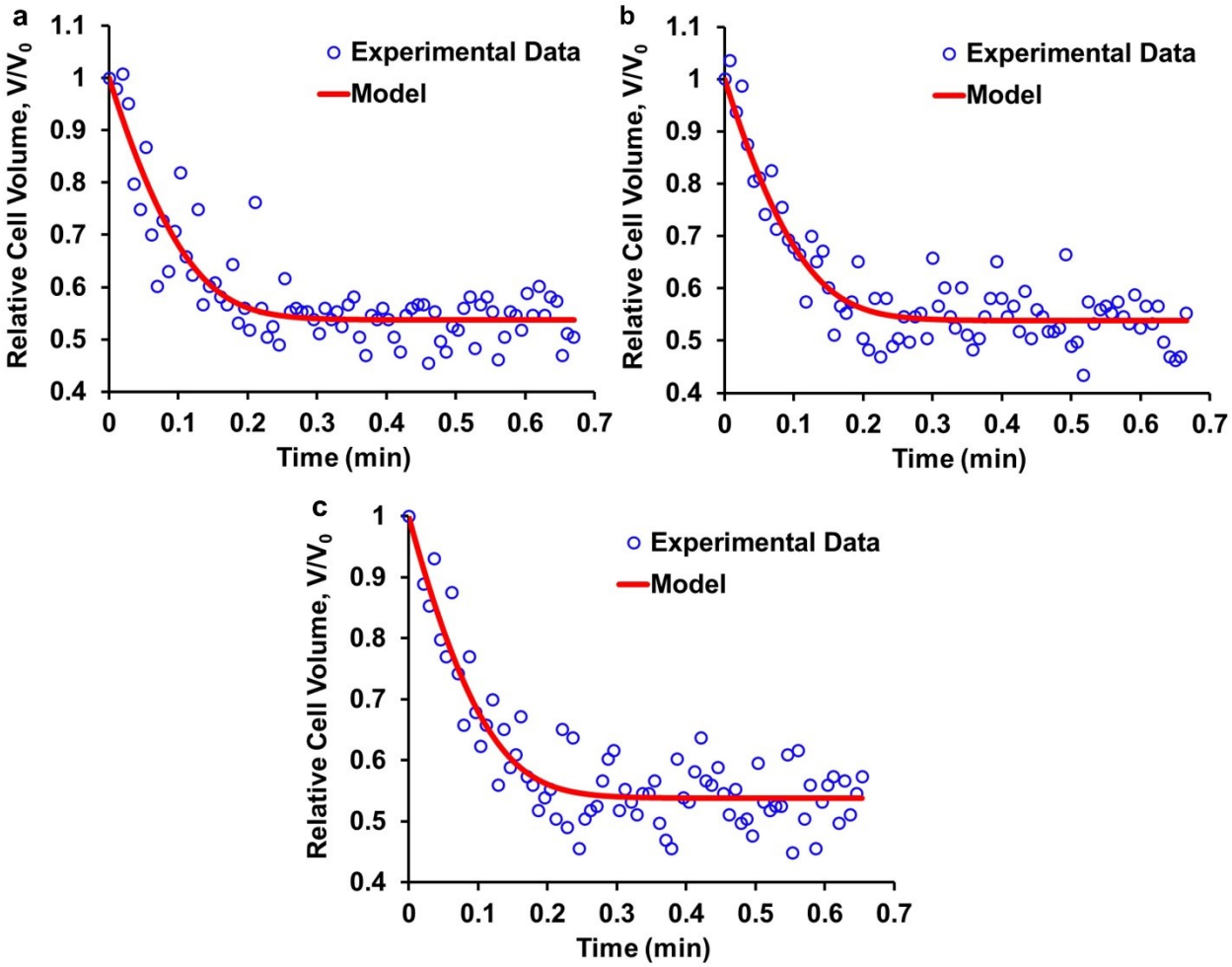

Figure A10. Separate fittings of 6x PBS runs using HUVECs at room temperature. Fitting parameters were L_p^{*RT} and b_{RT}^* using B_{gg} and C_{ggg} from the new fitting method. Run IDs: (a) H1024P61, (b) H1024P62, (c) H1024P64.

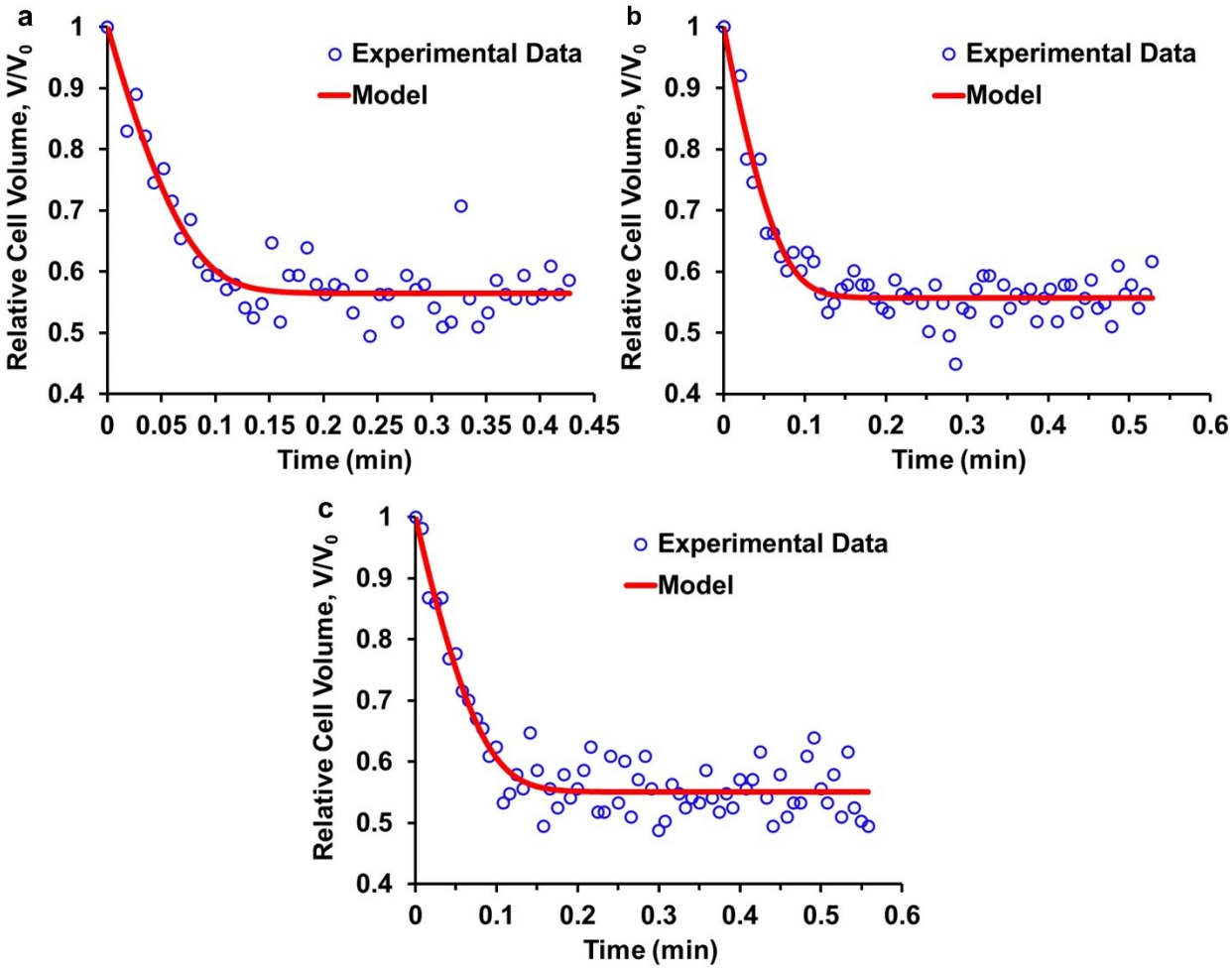

Figure A11. Separate fittings of 9x PBS runs using HUVECs at room temperature. Fitting parameters were L_p^{*RT} and b_{RT}^{*} using B_{gg} and C_{ggg} from the new fitting method. Run IDs: (a) H1025P92, (b) H1025P93, (c) H1025P94.

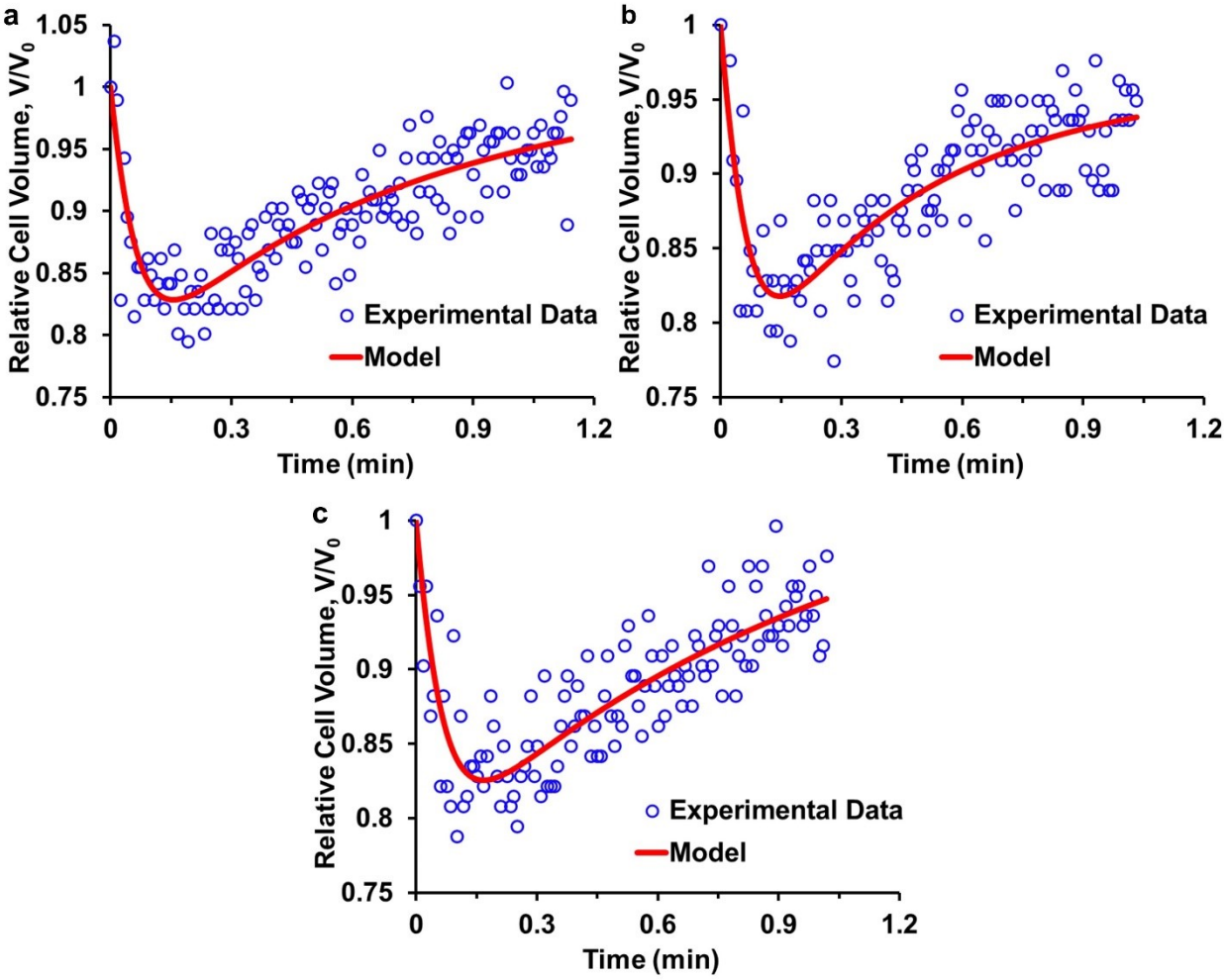

Figure A12. Separate fittings of 1 molal DMSO runs using HUVECs at room temperature. Fitting parameters were P_s^{*RT}, B_{gg}, and C_{ggg} using L_p^{*RT} and b_{RT}^{*} from the new fitting method. Run IDs: (a) H0221C12, (b) H0221C13, (c) H0221C14.

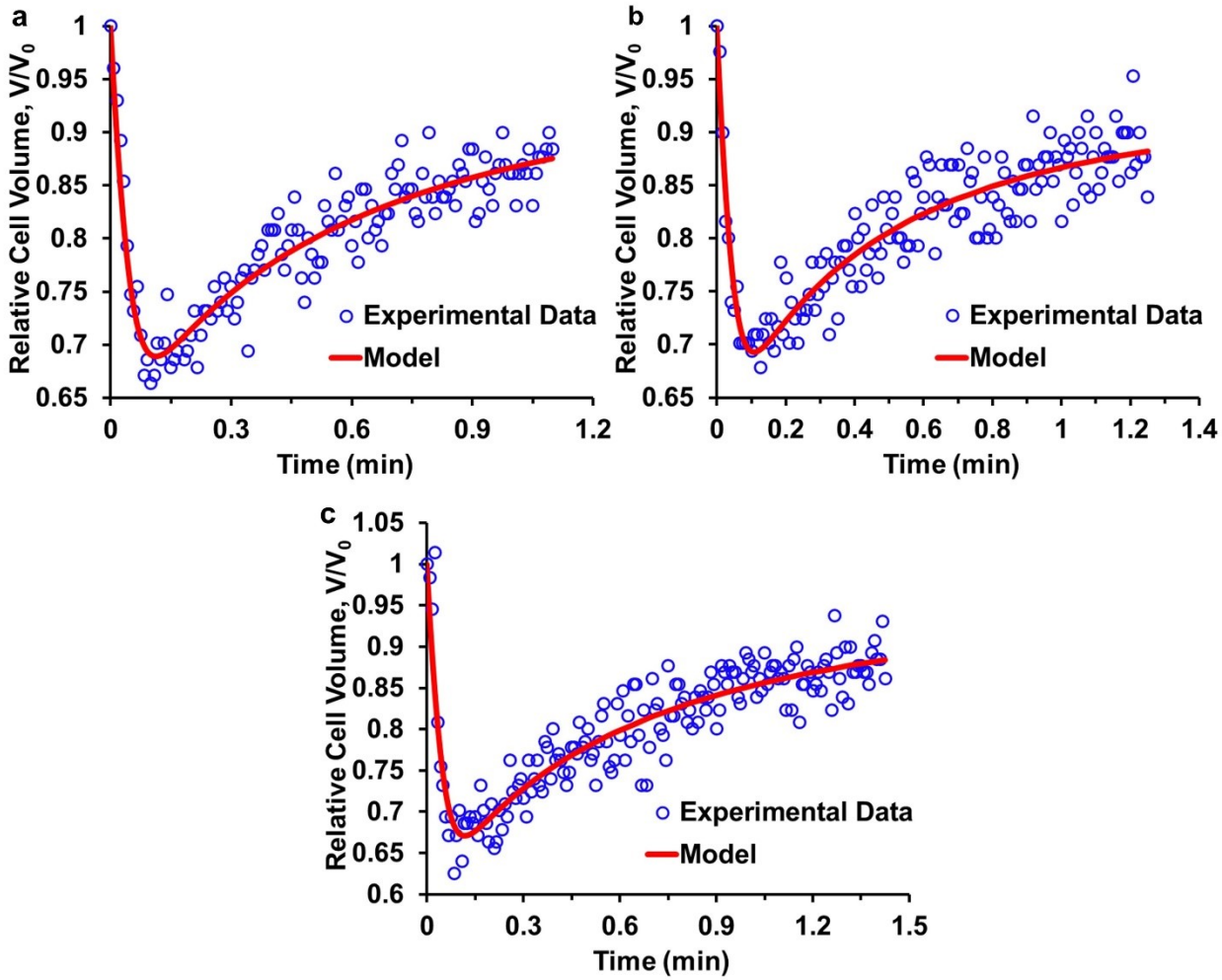

Figure A13. Separate fittings of 2 molal DMSO runs using HUVECs at room temperature. Fitting parameters were P_s^{*RT}, B_{gg}, and C_{ggg} using L_p^{*RT} and b_{RT}^* from the new fitting method. Run IDs: (a) H0225C22, (b) H0225C23, (c) H0225C24.

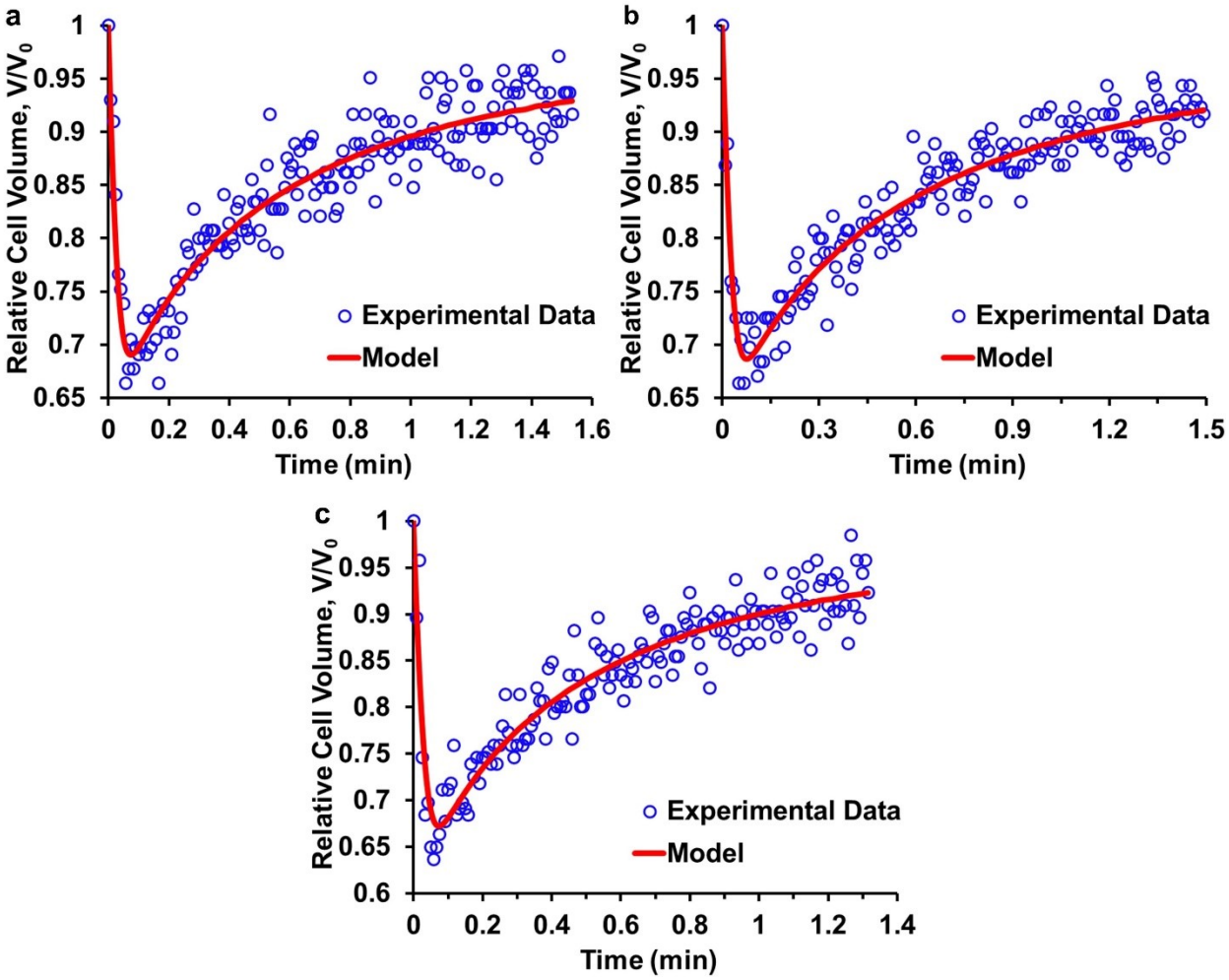

Figure A14. Separate fittings of 3 molal DMSO runs using HUVECs at room temperature. Fitting parameters were P_s^{*RT}, B_{gg}, and C_{ggg} using L_p^{*RT} and b_{RT}^* from the new fitting method. Run IDs: (a) H0228C31, (b) H0228C32, (c) H0228C33. Different from Figure A2 where the only fitting parameter was P_s^{*RT}.